Geochemistry Geophysics Geosystems G3
AN ELECTRONIC JOURNAL OF THE EARTH SCIENCES
Published by AGU and the Geochemical Society

Article
Volume 10, Number 10
24 October 2009
Q10012, doi:10.1029/2009GC002484
ISSN: 1525-2027

Click Here for Full Article

Global-scale quantification of mineralization pathways in marine sediments: A reaction-transport modeling approach

Martin Thullner
Department of Environmental Technology, UFZ, Helmholtz Centre for Environmental Research, Permoserstrasse 15, D-04318 Leipzig, Germany (martin.thullner@ufz.de)

Department of Earth Sciences–Geochemistry, Utrecht University, P.O. Box 80021, 3508 TA Utrecht, Netherlands

Andrew W. Dale
Leibniz Institute of Marine Sciences (IFM-GEOMAR), Wischhofstrasse 1-3, D-24148 Kiel, Germany

Pierre Regnier
Department of Earth Sciences–Geochemistry, Utrecht University, P.O. Box 80021, 3508 TA Utrecht, Netherlands

Department of Earth and Environmental Sciences, Université Libre de Bruxelles, 50 Avenue F. D. Roosevelt, B-1050 Brussels, Belgium

[1] The global-scale quantification of organic carbon (C_{org}) degradation pathways in marine sediments is difficult to achieve experimentally due to the limited availability of field data. In the present study, a numerical modeling approach is used as an alternative to quantify the major metabolic pathways of C_{org} oxidation (C_{ox}) and associated fluxes of redox-sensitive species fluxes along a global ocean hypsometry, using the seafloor depth (SFD) as the master variable. The SFD dependency of the model parameters and forcing functions is extracted from existing empirical relationships or from the NOAA World Ocean Atlas. Results are in general agreement with estimates from the literature showing that the relative contribution of aerobic respiration to C_{ox} increases from <10% at shallow SFD to >80% in deep-sea sediments. Sulfate reduction essentially follows an inversed SFD dependency, the other metabolic pathways (denitrification, Mn and Fe reduction) only adding minor contributions to the global-scale mineralization of C_{org}. The hypsometric analysis allows the establishment of relationships between the individual terminal electron acceptor (TEA) fluxes across the sediment-water interface and their respective contributions to the C_{org} decomposition process. On a global average, simulation results indicate that sulfate reduction is the dominant metabolic pathway and accounts for approximately 76% of the total C_{ox}, which is higher than reported so far by other authors. The results also demonstrate the importance of bioirrigation for the assessment of global species fluxes. Especially at shallow SFD most of the TEAs enter the sediments via bioirrigation, which complicates the use of concentration profiles for the determination of total TEA fluxes by molecular diffusion. Furthermore, bioirrigation accounts for major losses of reduced species from the sediment to the water column prohibiting their reoxidation inside the sediment. As a result, the total carbon mineralization rate exceeds the total flux of oxygen into the sediment by a factor of 2 globally.

Components: 14,256 words, 9 figures, 7 tables.

Keywords: early diagenesis; geomicrobiology modeling; redox reaction rates; terminal electron acceptor fluxes; carbon burial.

Copyright 2009 by the American Geophysical Union

Index Terms: 1051 Geochemistry: Sedimentary geochemistry; 1009 Geochemistry: Geochemical modeling (3610, 8410); 1055 Geochemistry: Organic and biogenic geochemistry.

Received 6 March 2009; **Revised** 6 August 2009; **Accepted** 14 August 2009; **Published** 24 October 2009.

Thullner, M., A. W. Dale, and P. Regnier (2009), Global-scale quantification of mineralization pathways in marine sediments: A reaction-transport modeling approach, *Geochem. Geophys. Geosyst.*, *10*, Q10012, doi:10.1029/2009GC002484.

1. Introduction

[2] Early diagenetic processes in marine sediments are of considerable importance for the global cycling of many elements at the Earth's surface. In sediments, the microbial degradation of organic carbon (C_{org}) is a dominant process that determines either directly or indirectly many other biogeochemical reactions [e.g., *Berner*, 1980; *Westrich and Berner*, 1984; *Middelburg*, 1989; *Boudreau and Ruddick*, 1991]. The complex interplay between the major redox cycles (carbon, oxygen, nitrogen, manganese, iron and sulfur) that is triggered by organic matter decomposition has been investigated at numerous sites worldwide with the aim of establishing global budgets [e.g., *Canfield*, 1993, *Tromp et al.*, 1995; *Jahnke*, 1996; *Seiter et al.*, 2005; *Hensen et al.*, 2006; *Jørgensen and Kasten*, 2006; *Zabel and Hensen*, 2006]. Yet, because of sampling difficulties and the complex pathways of early diagenesis, much of the available site specific benthic biogeochemical data do not provide sufficient information to describe the major carbon degradation processes. Perhaps more significantly, many sampling locations are not representative of the wider seafloor environment and are chosen on the basis of their unusual environmental characteristics. Thus, when extrapolated globally, these data sets introduce an unknown bias into C_{org} mineralization budgets.

[3] Various experimental methodologies have been proposed to quantify the flux of reactive particulate C_{org} from the surface layers down toward the seafloor. Direct estimations are obtained from export production and/or sediment trap deployments. Nonvertical particle settling and enhanced particle transport in benthic nepheloid layers can redistribute the benthic carbon oxidation demand over regional scales and so introduce large uncertainties in the final particle flux calculation [*Jahnke et al.*, 1990; *Reimers et al.*, 1992; *Inthorn et al.*, 2006]. More often indirect approaches are employed, based on (1) time change in total dissolved organic carbon (TCO_2) flux from sediments, which requires corrections for $CaCO_3$ dissolution [e.g., *Berelson et al.*, 1996], (2) dissolved oxygen uptake (DOU) by sediments using pore water O_2 microprofiles [e.g., *Glud et al.*, 1994], and (3) total oxygen uptake (TOU) by sediment from the time change in bottom water oxygen concentration [e.g., *Andersson et al.*, 2004]. The latter two methods are based on the premise that O_2 is the ultimate oxidant for C_{org} and reduced metabolites in the sediment resulting from anaerobic carbon mineralization. Of these, TOU probably represents the most robust way to gauge C_{org} flux because dissolved oxygen consumption by macrofauna [*Glud et al.*, 1994] and transport of reduced species (NH_4^+, Mn^{2+}, Fe^{2+}, H_2S), termed oxygen demand units (ODU) by *Soetaert et al.* [1996], can constitute a large fraction of total O_2 demand. However, if a significant fraction of ODU are buried as sedimentary sulfides or lost to the seawater and not corrected for, then TOU can potentially underestimate the depth-integrated rate of C_{org} mineralization. Perhaps not surprisingly, a combination of approaches and statistical analyses using various proxy parameters have been used to quantify spatially resolved C_{org} fluxes at the global scale [e.g., *Jahnke*, 1996; *Zabel and Hensen*, 2006; *Seiter et al.*, 2005].

[4] In the present study, we explore in more detail the global mineralization of C_{org} in the seafloor using a reaction-transport model (RTM) approach. RTMs simulate the complex interplay between transport processes and biogeochemical transformations, which allow for a temporally and spatially resolved quantification of reaction rates and material fluxes. In recent years, RTMs have become an established tool for the simulation of redox-sensitive processes in marine sediments [e.g., *Soetaert et al.*, 1996; *Boudreau*, 1996; *Van Cappellen and Wang*, 1996; *Dhakar and Burdige*, 1996; *Berg et al.*, 2003; *Thullner et al.*, 2005; *Dale et al.*, 2008a, 2008b]. We employ the seafloor depth (SFD) as the master variable for all simulations, which implies that the principal model parameters and semiempirically determined functions (boundary conditions, transport and reaction rate parameters) change from coastal shelf environments (100 m) to the deep ocean (5000 m) in a predictive manner. Statistically

Table 1. Subdivision of the Ocean Floor Into Depth Provinces[a]

	Depth Range (m)	Model SFD (m)	% Global
Inner shelf	0–150	100	5.8
Outer shelf	150–350	200	1.4
Upper slope	350–750	500	1.3
Midslope	750–1500	1000	2.6
Lower slope	1500–2750	2000	7.1
Abyss	2750–4250	3500	34
Abyss	>4250	5000	48
Global	—	—	3.3×10^{18} km^2

[a] Model simulations for each depth area are performed using boundary conditions and forcings corresponding to the model seafloor depth (SFD) indicated. The total seafloor area and percentages used in this study correspond to the ocean between 60°S and 60°N.

robust relationships developed by *Middelburg et al.* [1997] and *Meile and Van Cappellen* [2003] suggest that this condition is largely met throughout the ocean, yet these relationships have not been tested in global-scale models. The use of SFD as a master variable is attractive since, as *Middelburg et al.* [1997] remarked, SFD is an independent variable and free from experimental error, which is not true for the direct methodologies for carbon flux determination listed above. The approach does neglect regional-scale heterogeneity, which could be overcome by demarcation of the seafloor into biogeochemical provinces [*Longhurst et al.*, 1995]. However, our research interest in the present study is not to reproduce experimental data sets from specific sites or specific seafloor environments but first to compare the extent to which proposed SFD-dependent parameters support previous findings of global-scale POM mineralization and pathways along the global hypsometry. We will then investigate the fate and fluxes of ODUs generated in situ and discuss the validity of TOU as a proxy for organic carbon oxidation (C_{ox}) rate. To our knowledge, this will provide the first detailed analysis of source and sink fluxes for NH_4^+, Mn^{2+}, Fe^{2+} and H_2S in marine sediments at the global scale.

2. Simulation Procedure

2.1. Model Approach

[5] The RTM simulations are performed using boundary conditions and forcings corresponding to SFD of 100 m, 200 m, 500 m, 1000 m, 2000 m, 3500 m and 5000 m. These depths are representative of shelf, slope and abyssal sediments as described in Table 1. The relative contributions of each SFD interval to the total area of the seafloor are taken from the ETOPO5 5 × 5 min Navy bathymetry database [*National Geophysical Data Center*, 1993] available online (http://iridl.ldeo.columbia.edu/). The data analysis is restricted to latitudes between 60°S and 60°N and thus does not account for high latitude environments. These high latitudes represent only 13% of the global surface and ~10% of the total seafloor due to the relatively high abundance of landmasses at these latitudes.

[6] For each selected SFD, geochemical processes in the sediments are quantified using the Biogeochemical Reaction Network Simulator (BRNS) [*Regnier et al.*, 2002; *Aguilera et al.*, 2005], an adaptative simulation environment suitable for large, mixed kinetic-equilibrium reaction networks [e.g., *Thullner et al.*, 2005; *Jourabchi et al.*, 2005; *Dale et al.*, 2009]. For each dissolved species, i, the BRNS simulates the changes in pore water concentration, c_i, as a result of sediment burial, mixing due to molecular diffusion and bioturbation, bioirrigation, and species production/consumption due to reactions. If sediment compaction and porosity changes are neglected, the mass conservation equation for c_i, reads:

$$\frac{\partial c_i}{\partial t} = -v_{bur}\cdot\frac{\partial c_i}{\partial x} + \frac{\partial}{\partial x}\left(D_i^*\frac{\partial c_i}{\partial x}\right) + \frac{\partial}{\partial x}\left(D_b\frac{\partial c_i}{\partial x}\right) + \alpha\cdot\left(c_{i,0}-c_i\right) + R_i \quad (1)$$

[7] In equation (1), x and t are the vertical and temporal coordinates, v_{bur} is the burial velocity, D_i^* is the effective diffusion coefficient of species i, D_b is the bioturbation coefficient, α is the bioirrigation coefficient, $c_{i,0}$ is the dissolved concentration of at the sediment-water interface and R_i is the sum of all reaction rates consuming or producing species i. The spatial distributions of solid state species, l, are not influenced by molecular diffusion or bioirrigation and the mass conservation equation therefore reduces to:

$$\frac{\partial c_l}{\partial t} = -v_{bur}\cdot\frac{\partial c_l}{\partial x} + \frac{\partial}{\partial x}\left(D_b\frac{\partial c_l}{\partial x}\right) + R_l \quad (2)$$

where R_l is the sum of all reaction rates consuming and producing species l. R_i and R_l typically depend on other species concentrations than species i and l, respectively. Therefore, the reactions are coupled through the mass conservation equations (see below).

[8] Boundary conditions at the seafloor ($x = 0$) are specified as constant concentrations $c_{i,0}$ for dissolved species:

$$c_i(x=0) = c_{i,0} \quad (3)$$

Table 2. Processes and Variables Implemented in the Reaction Network

	Description
Reactions: Primary redox (C_{ox} reactions)	Organic matter degradation via aerobic respiration, denitrification, manganese reduction, iron reduction, sulfate reduction
Reactions: Secondary redox	oxidation of ammonium, sulfide, Mn(II) and Fe(II) by oxygen; oxidation of Fe(II) by Mn(IV); oxidation of sulfide by Mn(IV) and Fe(III); oxidation of FeS by oxygen
Reactions: Nonredox	precipitation/dissolution of Mn(II)- and Fe(II)-minerals; acid-base reactions (carbonate and sulfide system)
Variables	organic matter (solid); oxygen, nitrate, Mn(IV, solid), Fe(III, solid), sulfate; ammonium, Mn(II), Fe(II); Mn(II)- and Fe(II)- carbonate and sulfide minerals (solids); H^+, OH^-; H_2CO_3, HCO_3^-, CO_3^{2-}, H_2S, HS^-

and as a constant depositional flux, J_l (mass per seafloor area per unit time), for solid species:

$$J_l = \rho \cdot (1 - \Phi) \cdot \left(v_{bur} \cdot c_l - D_b \frac{\partial c_l}{\partial x} \right)_{x=0} \quad (4)$$

where ρ is the density of the solid matrix and Φ is the sediment porosity. At the lower boundary of the model domain (x_{max} = 50 cm), a zero gradient condition ($\partial c/\partial x = 0$) is applied for all species [*Boudreau*, 1997]. Specific values for all boundary conditions at the seafloor are discussed in section 2.3.2.

[9] Spatial discretization of equations (1) and (2) is performed using a one-dimensional finite difference scheme along an irregular grid composed of 111 nodes. The grid spacing increases from 1 mm at the sediment surface to 1 cm at x_{max}. Transient simulations are carried out until steady state is reached using a time step of 10^{-7} y for ocean margin sediments (SFD $\leq$ 1000 m) and 10^{-6} y for deep sea sediments (SFD > 1000 m). Mass balance in the system was always achieved with an accuracy of at least 0.1%.

2.2. Reaction Network and Definitions

[10] The reaction network implemented in the BRNS is taken from *Van Cappellen and Wang* [1995] and details on reaction stoichiometries, rate laws and equilibrium constraints can be found in Appendix A. In brief, the total C_{ox} rate, R_C, is simulated assuming a first order dependency with respect to labile particulate organic matter (POM), assumed to be $(CH_2O)_{106}(NH_3)_{12}(H_3PO_4)$. Other POM fractions which are not degraded within the 50 cm simulated domain are considered to be recalcitrant and not included in the simulations. The sequential contribution of the major metabolic pathways to the overall process of C_{org} decomposition (primary redox reactions) is controlled by empirical inhibition terms which ensure that $R_C = r_{O2} + r_{NO3} + r_{MnO2} + r_{FeOH3} + r_{SO4}$, where each $r\ldots$ denotes the rate of C_{ox} associated with a specific terminal electron acceptor (TEA). Secondary redox reactions, which mainly describe the reactions of the ODU produced by the primary reactions (NH_4^+, Mn^{2+}, Fe^{2+}, H_2S, and HS^-) are also included in the reaction network. Nonredox mineral precipitation/dissolution processes and acid base equilibria are considered (Table 2). Note that most model parameters which are associated with reactions not directly involved in C_{org} cycling are assumed to be independent or weakly sensitive to the SFD.

[11] The BRNS provides vertical profiles of individual species concentrations and reaction rates. From these profiles, the fluxes of dissolved species across the seafloor and (sediment) depth integrated reaction rates can be calculated. The depth-integrated C_{org} oxidation rate (mass per seafloor area per unit time) by each primary redox pathways, n, is simply obtained by depth integration over the whole model domain, x_{max}, which then allows calculating the total C_{ox} in the sediment:

$$C_{ox,total} = \sum_n \int_0^{x_{max}} r_n dx \quad (5)$$

In this study, the modeled sediment column is sufficiently large so that the labile carbon reaching the seafloor is completely degraded, i.e., there is no burial of labile C_{org} out of the last grid space in the model. Consequently, and considering that the ratio of carbon to oxygen during organic matter mineralization is 1:1 for a C_{org} oxidation state of zero, C_{org} flux in this study is assumed to be equivalent to the total oxygen uptake (TOU) of the sediment. We make this assumption because, in practical terms, TOU is normally considered to represent the depth integrated rate of C_{ox}, which

Table 3. SFD Dependency of Key Model Parameters and Boundary Conditions[a]

	Seafloor Depth						
	100 m	200 m	500 m	1000 m	2000 m	3500 m	5000 m
Model parameters							
v_{bur}[b] (cm yr^{-1})	3.98×10^{-1}	3.60×10^{-1}	2.67×10^{-1}	1.62×10^{-1}	5.94×10^{-2}	1.32×10^{-2}	2.94×10^{-3}
D_b[b] (cm^2 yr^{-1})	27.5	25.1	19.0	12.1	4.83	1.23	0.310
Φ[c]	0.85	0.85	0.80	0.80	0.80	0.80	0.80
α_0[d,e,f] (yr^{-1})	283	141	99.5	79.7	45.5	16.2	2.25
T[f] (°C)	10.3	9.7	8.1	5.8	3.0	1.5	1.4
S[f]	35	35	35	35	35	35	35
ρ[c] (g cm^{-3})[c]	2.5	2.5	2.5	2.5	2.5	2.5	2.5
k_C[g] (yr^{-1})[g]	0.221	0.208	0.174	0.130	0.0718	0.0296	0.0122
Upper boundary conditions							
$c_{O2,0}$[f] (μM)	132	129	121	114	116	135	141
$c_{NO3,0}$[f] (μM)	17.3	18.6	22.1	26.5	31.0	31.6	31.6
$c_{SO4,0}$[c] (mM)	28	28	28	28	28	28	28
J_{MnO2}[c] (μmol cm^{-2} yr^{-1})	1.35	1.20	0.840	0.464	0.141	2.38×10^{-2}	4.00×10^{-3}
J_{FeOH3}[c] (μmol cm^{-2} yr^{-1})	12.1	10.0	5.62	2.15	0.316	1.78×10^{-2}	1.00×10^{-3}
J_{POM}[b] (μmol cm^{-2} yr^{-1})	510	467	357	228	93.0	24.3	6.33
pH[c]	8.1	8.1	8.1	8.1	8.1	8.1	8.1
Alkalinity[c] (meq L^{-1})	2.4	2.4	2.4	2.4	2.4	2.4	2.4

[a] The upper boundary conditions for the other variables are specified either as zero concentration or as zero fluxes for dissolved and solid species, respectively. All other parameters are summarized in Table A3.
[b] Derived/adapted from *Middelburg et al.* [1997].
[c] Derived/adapted from *Van Cappellen and Wang* [1995].
[d] Derived/adapted from *Meile and Van Cappellen* [2003].
[e] Derived/adapted from *Andersson et al.* [2004].
[f] Derived/adapted from *Conkright et al.* [2002].
[g] Derived/adapted from *Boudreau* [1997].

requires that all the ODU produced from the primary redox reactions are oxidized back to MnO_2, $Fe(OH)_3$, SO_4^{2-} using O_2 as the ultimate TEA. Strictly, however, TOU is not equal to the flux of C_{org} remineralized in the seafloor for three reasons. First, some ODU escape reoxidation and are buried in the long term sedimentary record, mainly as particulate iron sulfides, and a correction to measured TOU may be necessary [*Berelson et al.*, 1996]. Second, if all POM were to be degraded by denitrification, then the TOU will be zero since the N_2 product is not oxidized in the sediment or bottom water. Third, POM contains particulate organic nitrogen (PON), represented by NH_3. In our model, aerobic respiration is described as coupled oxidation and nitrification (Tables A1 and A2 in Appendix A) where PON is oxidized directly to NO_3^-. Thus, if all POM were to be degraded aerobically, the TOU demand would be 1.22 times greater than TOU calculated on a carbon-only basis. Between these two end-member cases, other TOU values can be obtained when the oxidation of the NH_4^+ released during manganese, iron and sulfate reduction is not complete. Nonetheless, to avoid these complications and allow a more straightforward comparison with literature data, TOU in this study refers to the POC component of POM only:

$$TOU = J_{POC} \tag{6}$$

For similar reasons, we exclude NH_4^+ from the calculation of ODU:

$$J_{ODU} = \frac{1}{2} \cdot J_{Mn^{2+}} + \frac{1}{4} \cdot J_{Fe^{2+}} + 2 \cdot J_{H_2S} \tag{7}$$

and NH_4^+ fluxes are discussed separately. Note that in equation (7) H_2S corresponds to total dissolved sulfide ($H_2S + HS^-$).

2.3. SFD-Dependent Parameters

[12] This section describes the general SFD dependency of all model parameters directly involved in C_{org} decomposition. A summary of all values selected for the variables, parameters and boundary conditions along the global hypsometry is given in Table 3. In the empirical relationships presented below the SFD is specified in meters (m).

2.3.1. Transport Parameters

[13] The global-scale relationship between burial velocity v_{bur} (cm yr^{-1}) and SFD is taken from the statistically significant (r^2 = 0.615, n = 220, p = 0.0000) empirical relationship of *Middelburg et al.* [1997] (there presented as sediment accumulation rate):

$$v_{bur} = 3.3 \cdot 10^{-(0.8748-0.0004351 \cdot \mathrm{SFD})} \quad (8)$$

[14] The bioturbation coefficient D_b (cm^2 yr^{-1}) is similarly expressed as [*Middelburg et al.*, 1997]:

$$D_b = 5.2 \cdot 10^{(0.7624-0.0003972 \cdot \mathrm{SFD})} \quad (9)$$

D_b values used in the regression analysis by *Middelburg et al.* [1997] are based on ^{210}Pb measurements and depend significantly on SFD (r^2 = 0.432, n = 132, p = 0.0000). Studies suggest that the surface sediment mixed by bioturbation is approximately 10 cm thick and independent of the SFD [*Boudreau*, 1997; *Van Cappellen and Gaillard*, 1996]. Based on these results, a mixed layer depth of 10 cm is imposed for all simulations, an assumption generally supported by the more recent study of *Teal et al.* [2008], who presented a mixed layer depth of 6 ± 6 cm with only marginal dependency on SFD.

[15] The effective diffusion coefficient D_i* (cm^2 yr^{-1}) for each dissolved species i is given by:

$$D_i^* = \frac{D_i(\mathrm{T},\mathrm{S})}{1 - \ln(\Phi^2)} \quad (10)$$

where $D_i(T, S)$ (cm^2 yr^{-1}) is the species-dependent, molecular diffusion coefficient in seawater at a given temperature (T) and salinity (S) [*Boudreau*, 1997]. D_i* also depends on SFD through T (see below) and Φ. Values of Φ are set to 0.85 for SFD $\leq$ 200 m and to 0.80 for SFD $\geq$ 200 m [*Van Cappellen and Wang*, 1995].

[16] The bioirrigation rate α (yr^{-1}) is calculated from the bioirrigation coefficient at the sediment surface (α_0, yr^{-1}) and the bioirrigation attenuation depth length (x_{irr}, cm):

$$\alpha = \alpha_0 \cdot \exp(-x/x_{irr}) \quad (11)$$

Due to a lack of data, x_{irr} is assumed to be independent of the SFD and set to 3.5 cm. This irrigates the sediment down to ~15 cm depth, which although typical for shelf sediments [*Van Cappellen and Wang*, 1996; *Meile et al.*, 2001; *Burdige*, 2006] may not be so for deeper environments. We discuss the ramifications of this approach below. We also assume that irrigation rates are identical for all species, although we recognize that some highly redox sensitive species such as Fe^{2+} may be irrigated at much lower rates due to oxidation at the walls of animal burrows [*Meile et al.*, 2005]. α_0 is calculated from the mean bioirrigation coefficient in the aerobic sediment layer ($\overline{\alpha}$, yr^{-1}) and the penetration depth of O_2 into the sediment (x_{O2}, cm) [*Meile and Van Cappellen*, 2003]:

$$\alpha_0 = \frac{\overline{\alpha} \cdot x_{O2}}{x_{irr} \cdot \left(1 - \exp\left({}^{x_{O2}}/_{x_{irr}}\right)\right)} \quad (12)$$

where

$$\overline{\alpha} = \frac{-73.071 + 71.912 \cdot \exp(-0.0013846 \cdot J_{O2})}{c_{O2}/1000} \quad (13)$$

$$x_{O2} = 0.5 \cdot \frac{2 \cdot \Phi \cdot c_{O2} \cdot D_{O2}^*}{J_{O2,diff}} + 0.5 \cdot \frac{2 \cdot \Phi \cdot c_{O2} \cdot D_{O2}^*}{\left(J_{O2,diff}\right)^2} \cdot J_{O2} \quad (14)$$

In equation (13) and (14), J_{O2} (μmol cm^{-2} yr^{-1}) and $J_{O2,diff}$ (μmol cm^{-2} yr^{-1}) are defined as the total flux and the diffusive flux of O_2 across the sediment-water interface, respectively, c_{O2} (μM) is the bottom water O_2 concentration, and the noninteger coefficients are empirically derived by *Meile and Van Cappellen* [2003].

[17] J_{O2} is directly dependent on the SFD [*Wijsman*, 2000; *Andersson et al.*, 2004]:

$$J_{O2} = J_0[(1-p) \cdot \exp(-b_1 \cdot \mathrm{SFD}) + p \cdot \exp(-b_2 \cdot \mathrm{SFD})] \quad (15)$$

where J_0 is equal to J_{O2} for SFD = 0 (986 μmol cm^{-2} yr^{-1}), p is a partitioning coefficient of J_0, equal to 0.14, and b_1 (0.017 m^{-1}) and b_2 (0.00047 m^{-1}) control the slopes of the exponentials (values taken from *Wijsman* [2000]). This relationship (r^2 = 0.71) is derived from more than 500 TOU estimates measured for SFD between 10 and 9000 m.

[18] Finally, $J_{O2,diff}$ in equation (14) is derived from J_{O2} using the empirical relation derived by *Meile and Van Cappellen* [2003] based on a comparison of measured O_2 fluxes calculated by O_2 micro-

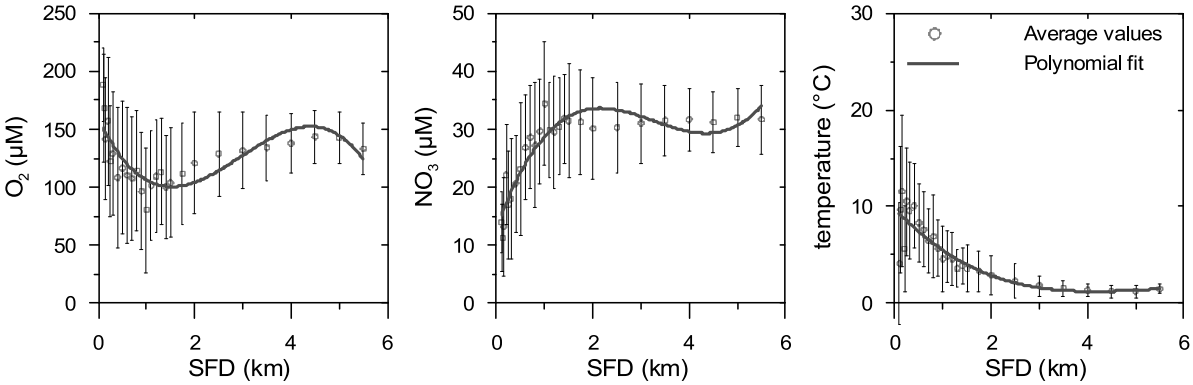

Figure 1. Imposed boundary conditions for O_2, NO_3^-, and temperature. Symbols and error bars show averages and standard deviations of global values.

sensor profiles and in situ benthic chamber incubations ($n = 41$, $r^2 = 0.79$):

$$J_{O2,diff} = \frac{500 \cdot J_{O2}}{646 + J_{O2}} \quad (16)$$

Table 3 shows that α_0 decreases by 2 orders of magnitude between 100 m and 5000 m, which reflects the lower availability of labile C_{org} with increasing SFD.

2.3.2. Upper Boundary Conditions

[19] Values for O_2, NO_3^-, T and S are taken from the NOAA World Ocean Atlas 2001 [*Conkright et al.*, 2002], available online at the IRI/LDEO Climate Data Library (http://iridl.ldeo.columbia.edu/). In this database, the variables are reported with a 1° × 1° horizontal resolution and a vertical resolution which varies from 10 m close to the sea surface to 500 m for water depths >2000 m, up to a maximum depth of 5500 m. In the present study, the annual mean data recorded at the deepest water depth for any given horizontal coordinate is assumed to be representative of the seafloor conditions at this coordinate. Average bottom water values of O_2 (μM), NO_3^- (μM), T (°C) and S are then calculated for each SFD interval as indicated by the polynomial data interpolation in Figure 1. Even though the data show a considerable degree of variability due to basin-wide differences in water masses, the interpolations capture the essential features such as the oxygen minimum zone on the continental slope. Due to the low variability with SFD, sulfate (SO_4^{2-}) and S along the global hypsometry were fixed to 28 mM and 35 for all simulations, respectively. For both S and T, the upper boundary condition is applied over the entire sediment core.

[20] The flux of POM reaching the seafloor which is mineralized in the upper 50 cm is derived from the empirical relationship of *Middelburg et al.* [1997] between carbon mineralization rate and SFD ($r^2 = 0.69$, $n = 80$, $p = 0.0000$). These authors split the total flux of POM reaching the seafloor into a nonreactive fraction that is buried and a degradable fraction that is mineralized (both fractions having similar magnitudes at the global scale). Assuming that the carbon mineralization rate provides a realistic estimate of the flux of degradable POM reaching the seafloor (J_{POM}, μM C cm^{-2} yr^{-1}), J_{POM} can be quantified by:

$$J_{POM} = 1800 \cdot 10^{(-0.5086 - 0.000389 \cdot SFD)} \quad (17)$$

[21] Note that for water depths >1000 m, J_{POM} values predicted by equation (17) are in good agreement with the more recent sediment TOU curve developed by *Andersson et al.* [2004]. Higher fluxes are predicted by equation (17) for shallower water depths, which probably results from the different regression techniques employed in the two studies.

[22] Although the distribution of reducible manganese and iron in marine sediments is well documented at many individual sites [e.g., *Canfield et al.*, 1993; *Aller*, 1994; *Slomp et al.*, 1997], no estimate is currently available to constrain the deposition flux of the particulate metal oxide along the global hypsometry. We assume that the fluxes for 200 m and 5000 m SFD can be approximated by those derived from previous model studies for shelf and deep sea sediments, respectively [*Van Cappellen and Wang*, 1995]. Extrapolation to intermediate SFD is then obtained by exponential interpolation. Sensitivity analysis (not shown) revealed that the model output is insensitive to either an exponential or linear interpolation func-

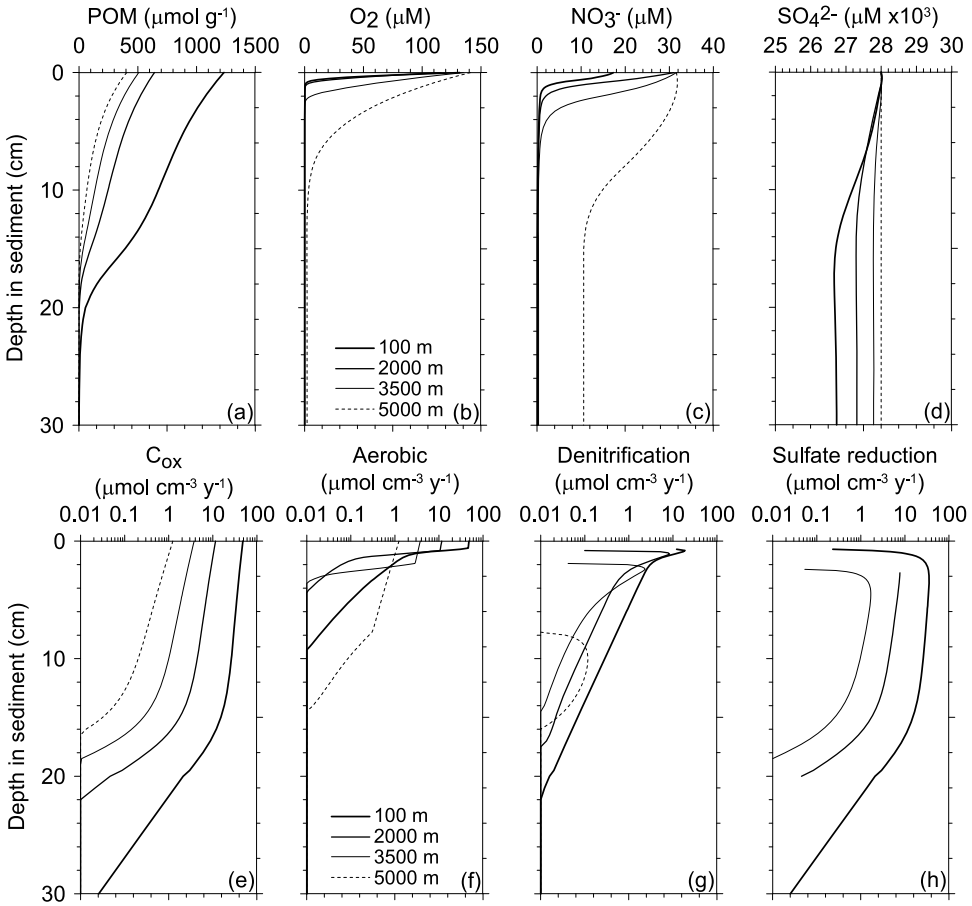

Figure 2. Model profiles of (a) POM, (b) O_2, (c) NO_3^-, and (d) SO_4^{2-} concentration with depth in the sediment and modeled rates of (e) organic carbon oxidation (C_{ox}), (f) aerobic respiration, (g) denitrification, and (h) sulfate reduction rates (all rates given in carbon equivalents). Profiles are provided for SFD of 100, 2000, 3500, and 5000 m.

tion. In view of the uncertainty in constraining the fluxes of Mn and Fe oxides to the seafloor and as using original flux values from *Van Cappellen and Wang* [1995] led to negligible contribution of these pathways to total POM, these original values are arbitrarily increased by a factor of 100 to increase their sensitivity on POM degradation rates.

2.3.3. Rate of POM Degradation

[23] The oxidation of POM is simulated using a 1-G model approach [*Berner*, 1980], which assumes a single pool of degradable organic matter of uniform reactivity, described by first order kinetics with respect to POM. The rate constant, k_C (yr^{-1}), is obtained from *Boudreau* [1997] using an expression relating k_C to v_{bur}:

$$k_C = 0.38 \cdot v_{bur}^{0.59} \tag{18}$$

This rate constant is applicable to the more reactive carbon fractions which are degraded within the top 10–20 cm of sediments and more recalcitrant fractions are not considered. As Boudreau admits, this relationship may be biased toward the type of environmental settings from where the data originate. We nonetheless choose to employ this relationship since it is our prime interest to observe how this type of simple relationship impacts carbon degradation globally. Possible artifacts are discussed further below.

3. Results and Discussion

3.1. Concentration and Rate Distributions

[24] Simulated depth concentration profiles of POM, O_2, NO_3^- and SO_4^{2-} for 100, 2000, 3500 and 5000 m are shown in Figures 2a–2d, and respiration pathways are shown in Figures 2e–2h. As expected, the highest surface POM concentrations are found at 100 m water depth (1200 μmol g^{-1}) compared to the deep ocean (400 μmol g^{-1}). The POM concentration profiles do not reproduce residual POM concentrations since recalcitrant POM pools are not included and assumed to be nonreactive within the 50 cm model domain. In

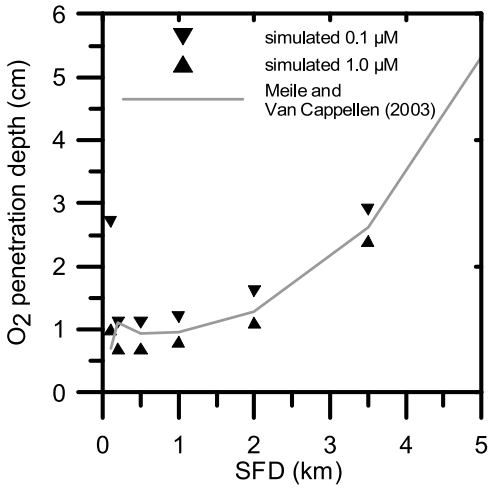

Figure 3. O_2 penetration depths as a function of SFD. For the simulations two different threshold concentrations (0.1 μM and 1.0 μM) are used to indicate complete O_2 depletion. At 5 km SFD, the simulated O_2 concentrations are always above 1.0 μM. The results from *Meile and Van Cappellen* [2003] were obtained combining equations (14) to (16).

general, the flux of POM to the seafloor, which decreases by 2 orders of magnitude from 100 to 5000 m (Table 3), has a greater impact on POM concentrations than its reactivity, which decreases by only 1 order of magnitude. Yet, bioturbation is clearly an important transport mechanism for mixing reactive POM down below the oxic layer where burial velocities in the deep ocean are extremely low (Table 3). For all water depths, the POM concentration is reduced by > 99% of the surface concentration by 30 cm depth.

[25] The rate of POC mineralization (C_{ox}) is around 50 times greater at 100 m than at 5000 m (Figure 2e). The model-derived rate profiles in Figures 2f–2h show that aerobic respiration is the main pathway for POM degradation if O_2 is present (Figure 2b), which is a direct result of the inhibition of carbon degradation by other electron acceptors if O_2 is above 8 μM (see Appendix A). The spatial domain of aerobic respiration increases from <1 cm at 100 m SFD to > 10 cm at 5000 m SFD. The large oxygen penetration depths are typical for deep water sediments [*Glud et al.*, 1994; *Glud*, 2008]. Simulated oxygen penetration depths also agree well with the global-scale predictions of *Meile and Van Cappellen* [2003] (Figure 3). Only, at 5000 m SFD, *Meile and Van Cappellen* [2003] predict a large (>5 cm), yet finite oxygen penetration depth whereas our model predicts oxygen throughout the sediment at very low concentrations. A likely explanation for this artifact is the simulation of a single labile POM pool only. Furthermore, in these deep waters, NO_3^- also persists throughout the sediment and inhibits sulfate reduction (Figure 2c). The zone of denitrification extends from about 8–16 cm in the deep ocean and overlaps the zone of aerobic respiration (Figure 2g). The subsurface preponderance of oxic and suboxic conditions is a characteristic feature of deep sea sediments [e.g., *Jørgensen*, 1982; *Canfield*, 1989; *Tromp et al.*, 1995; *Jørgensen and Kasten*, 2006]. Although barely discernible in Figure 2, in situ production of NO_3^- from biogenic nitrogen causes a slight increase in NO_3^- with depth below the sediment surface (Figure 2c). This simulated effect is in agreement with experimental observations, which show that the subsurface increase in NO_3^- may be even more pronounced. For example, in the deep Pacific Ocean the subsurface NO_3^- increase is > 20 μM within 2 cm below the seafloor [*Berelson et al.*, 1990]. The small increase in NO_3^- in the model simulation results could be because our bottom water O_2 concentration at 5000 m (150 μM) is lower than measured in the Pacific Ocean.

[26] When NO_3^- is exhausted, sulfate reduction is the main pathway for POM mineralization with decreasing rates with increasing water depth (Figure 2h). Overall, the simulated shift from predominant sulfate-based carbon mineralization to aerobic respiration with increasing SFD is in qualitative agreement with field evidence [e.g., *Canfield*, 1989; *Cai and Reimer*, 1995; *Thamdrup and Canfield*, 1996; *Jahnke*, 1996; *Ferdelman et al.*, 1999; *Canfield et al.*, 2005] and earlier modeling studies [*Van Cappellen and Wang*, 1995; *Tromp et al.*, 1995; *Soetaert et al.*, 1996]. It is also interesting to observe that, with the exception of the deep abyss (>4250 m, Table 1), downward mixing of labile carbon stimulates sulfate reduction within the mixed layer despite the very low bioturbation rates (1.2 $cm^2\ yr^{-1}$, Table 3). In all cases, SO_4^{2-} concentration remains above 26 mM (Figure 2d) in the simulated sediment column. In nature it is likely that sulfate concentrations will further decrease with sediment depth due to the oxidation of refractory organic carbon in deeper sediment layers, a process not considered in this study.

[27] Note that on the axes scales of the plots, the depth of aerobic respiration and denitrification consistently exceed the apparent depth of O_2 and NO_3^- penetration, although the rates do show a dramatic decrease below the observed penetration depth (Figures 2b and 2f). Solutes are transported to these deeper sediments by bioirrigation, and the incongruities in the concentration and rate profiles are due to rapid turnover of O_2 and NO_3^-. *Meile et*

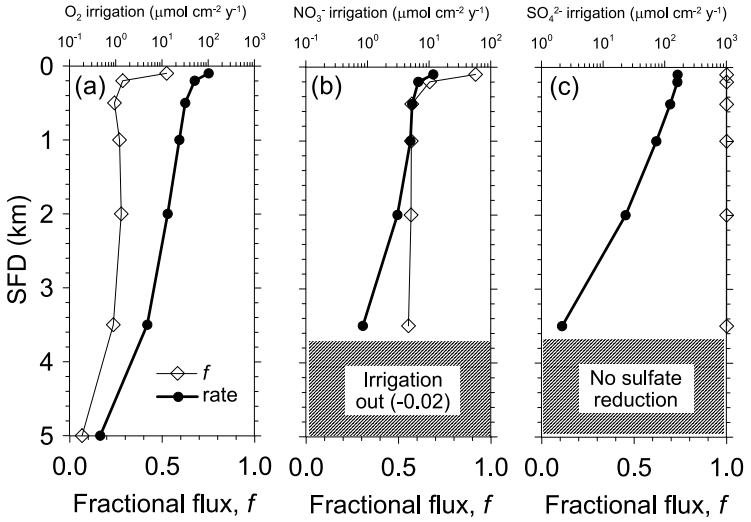

Figure 4. Model-predicted rates of (a) O_2, (b) NO_3^-, and (c) SO_4^{2-} bioirrigation fluxes into the sediment and the fraction of total influx due to bioirrigation.

al. [2001] calculated that only 10–20% of total O_2 influx is delivered to the aerobic zone, with the remainder being transported by nonlocal mechanisms to greater depths. Overall, the relative importance of bioirrigation to the total solute flux to the sediment is largest at 100 m SFD for O_2 and NO_3^- where it contributes ~50% and 90% of the total flux into the sediment, respectively (Figures 4a and 4b). TOU:DOU ratios above 1 are characteristic of sediments receiving high fluxes of labile carbon [*Seiter et al.*, 2005]. Between 200 m and 3500 m, the relative importance of bioirrigation is much lower for O_2 (25%) and NO_3^- (60%), and at 5000 m, it accounts for <10% of total O_2 influx. This agrees with *Glud et al.* [1994], who showed that that depth-integrated O_2 consumption is not statistically different from DOU in deep sea sediments. No data are plotted for NO_3^- for the deep abyssal sediments because the net solute flux of NO_3^- is to the ocean (Figure 2c) [*Hammond et al.*, 1996; *Hensen et al.*, 1998].

[28] Bioirrigation is even more important for SO_4^{2-} and accounts for all of the input throughout the ocean (Figure 4c). Even though this may not be wholly representative of coastal sites where highly reactive POM fractions drive a larger diffusive flux gradient, bioirrigation is still a major transport pathway for SO_4^{2-}. Recent modeling studies of coastal sediments calculate that 80–90% of SO_4^{2-} transport into the sediment from the seawater occurs through nonlocal processes [*Dale et al.*, 2008a, 2008b]. The increasing importance of bioirrigation to the total rate of solute input follows the order $SO_4^{2-} > NO_3^- > O_2$ which generally reflects their depth of consumption by C_{ox}. For example, aerobic respiration begins immediately at the sediment-water interface, which induces a steeper concentration gradient and, consequently, a higher diffusive flux than both NO_3^- and SO_4^{2-}. The latter is not consumed in the uppermost sediment layers and displays much more vertical concentration gradients (Figure 2d). Transport into the sediment must therefore be dominated by irrigation.

3.2. Global Hypsometric Analysis of TEA Fluxes and C_{ox} Rates

[29] Simulated depth-integrated C_{ox} rates (μmol C cm^{-2} yr^{-1}) by the primary redox pathways along the global hypsometry are shown in Figures 5a–5e, and the corresponding total fluxes of dissolved (O_2, NO_3^- and SO_4^{2-}) and solid (MnO_2 and $Fe(OH)_3$) TEAs to the sediment directly from the ocean are shown below in Figures 5f–5j in terms of carbon oxidation potential (μmol C cm^{-2} yr^{-1}). TOU is also compared in Figure 5f to the empirical TOU-SFD relationship derived by *Andersson et al.* [2004]. The solute fluxes are driven by the chemical gradients in the sediment through bioirrigation and diffusion, whereas the solid fluxes are directly determined by the applied boundary conditions.

[30] The C_{ox} rates by each pathway display a decrease with SFD, with the exception of MnO_2 reduction which displays an unusual behavior owing to secondary redox cycling (Figures 5a–5e). The decrease is consistent with the imposed decrease of POM flux and reactivity with increasing SFD (Table 3). Observational data for comparison, which are taken from the database compiled by *Middelburg et al.* [1996, 1997], are only available for aerobic respiration, denitrification and sulfate reduction

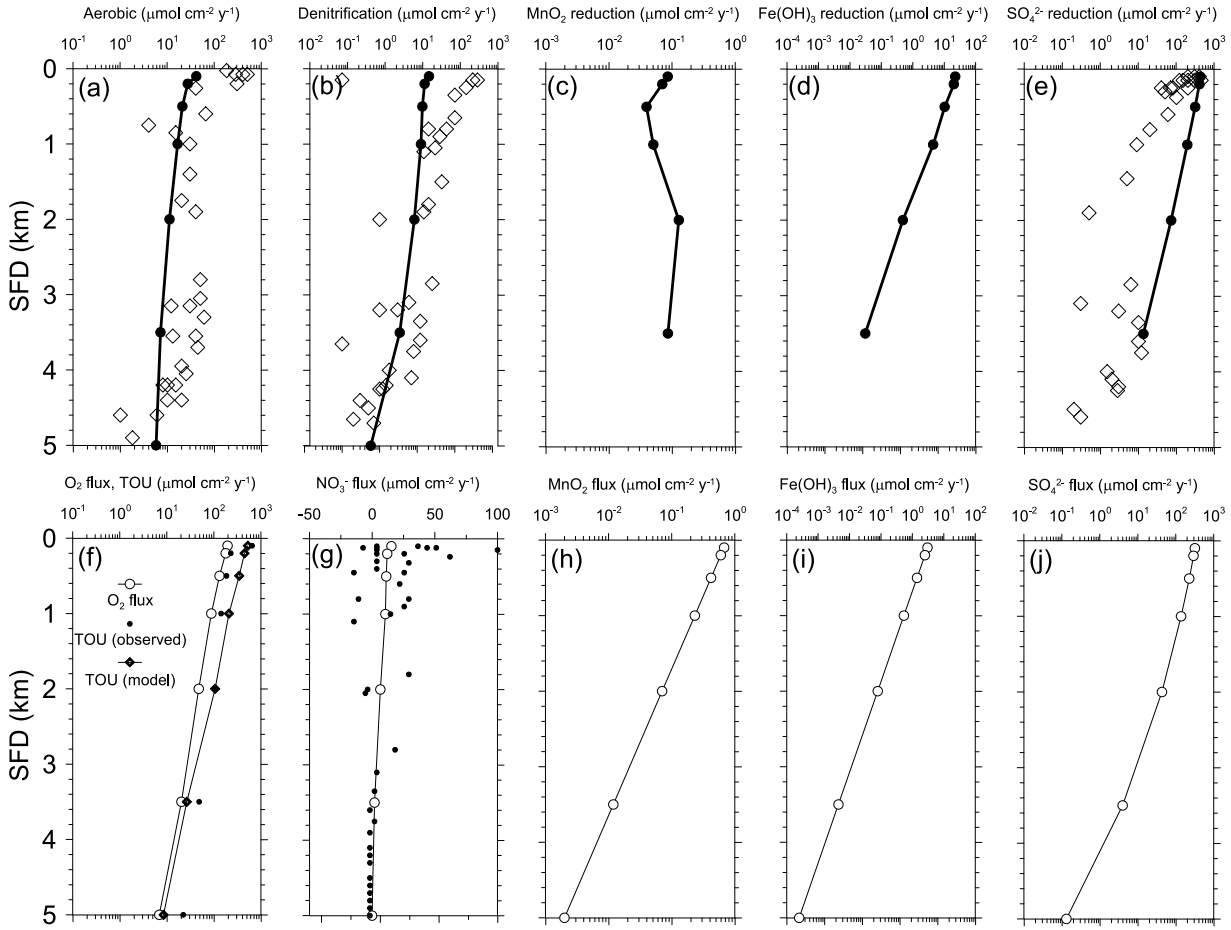

Figure 5. (a–e) Modeled (lines) profiles of carbon mineralization rates along the global hypsometry and (f–j) modeled (lines, open symbols) fluxes of O_2, NO_3^-, metal oxides, and SO_4^{2-} to the sediment (the rates are converted to carbon units using the stoichiometry of POC degradation; see Appendix A). The diamonds in Figures 5a, 5b, and 5e represent observations taken from the database compiled by *Middelburg et al.* [1997]. Also plotted in Figure 5f are the TOU estimates using the relationship of *Andersson et al.* [2004] (denoted "TOU (observed)") and POC flux in this study (≡TOU) (denoted "TOU (model)"). The points in Figure 5g are observed NO_3^- fluxes taken from *Middelburg et al.* [1996].

(Figures 5a, 5b, and 5e). For the shelf sediments (0–350 m water depth), the agreement between the model and observations is favorable for sulfate reduction, but less favorable for aerobic respiration and denitrification whereby the model predicts lower values by up to 200–400 μmol cm^{-2} yr^{-1}. Note that the average sum of measured rates of aerobic respiration, denitrification and sulfate reduction for the shelf (~900 μmol C cm^{-2} yr^{-1}; Figures 5a, 5b, and 5e) is much higher than the total carbon mineralization rate reported in the same database. The latter is ~500 μmol cm^{-2} yr^{-1} [*Middelburg et al.*, 1997], which compares well to our modeled TOU mineralization rate (Figure 5f). A similar mineralization rate of 400 μmol cm^{-2} yr^{-1} is also predicted by predicted by the model of *Andersson et al.* [2004] (Figure 5f)

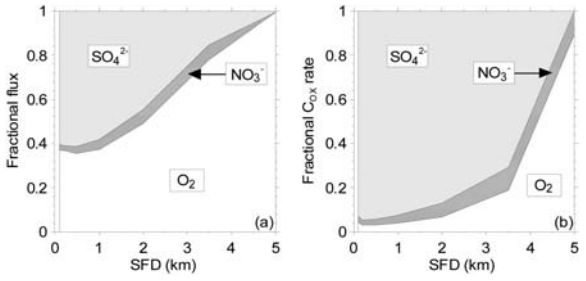

Figure 6. (a) The relative contribution of O_2, NO_3^-, and SO_4^{2-} to the total flux of TEAs into the sediment (expressed as a fraction of the total carbon oxidation capacity). (b) The relative contribution of aerobic respiration, denitrification, and sulfate reduction to C_{ox}. Manganese and iron oxide play a negligible role and are not shown.

Table 4. Global and Hypsometric Fluxes of Total Oxygen Uptake, Oxygen Demand Units, Terminal Electron Acceptors, Global Primary Redox Rates[a]

	TOU	ODU Flux	O_2 Flux	NO_3^- Flux	$Fe(OH)_3$ Flux	SO_4^{2-} Flux	Aerobic Respiration	Denitrification	Iron Reduction	Sulfate Reduction
Inner shelf (0–150 m)	45%	56%	35%	31%	70%	61%	28%	29%	68%	52%
Outer shelf (150–350 m)	10%	13%	8.1%	6.0%	14%	13%	4.3%	5.4%	15%	12%
Upper slope (350–750 m)	7.4%	8.5%	5.6%	5.4%	7.5%	8.8%	2.9%	4.4%	7.3%	8.5%
Midslope (750–1500 m)	9.2%	10%	7.3%	11%	5.6%	9.4%	3.9%	8.4%	6.2%	10%
Lower slope (1500–2750 m)	10%	8.5%	11%	22%	2.2%	6.0%	6.0%	16%	1.8%	9.9%
Abyss (2750–4250 m)	13%	3.5%	22%	26%	0.6%	1.7%	24%	30%	0.6%	7.0%
Abyss (>4250 m)	4.7%	0.0%	11%	−1.7%	0.0%	0.2%	31%	6.7%	0.0%	0.0%
Global (Tmol yr^{-1})	21	11	10	0.7	0.33	5.5	3.1	1.3	0.6	16

[a] TOU, total oxygen uptake (mol O_2); ODU, oxygen demand units (mol O_2), TEA, terminal electron acceptors (mol TEA); global primary redox rates (mol C). All numbers are rounded to 2 significant figures. Data for manganese are typically 10% of the values of iron and are not shown. The percentages refer to the fraction of the total global flux or rate listed in the bottom row. Note that TOU is defined as the carbon-containing portion of POM $[(CH_2O)_{106}(NH_3)_{12}(H_3PO_4)]$ (as determined by the boundary conditions) and does not include the O_2 demand from liberated biogenic nitrogen (NH_4^+). The ODU flux is defined as the total flux of reduced metabolites (N_2, Mn^{2+}, Fe^{2+}, H_2S) out of the sediment excluding NH_4^+.

for SFD of 0–350 m. When considered collectively, our model provides a good correspondence for TOU at these water depths compared to *Middelburg et al.* [1997] and *Andersson et al.* [2004].

[31] The modeled data in Figure 5 are summarized in Figure 6a and Figure 6b as the fractional contribution of each dissolved TEA (O_2, NO_3^-, SO_4^{2-}) to the total electron acceptor flux and C_{ox} rate as a function of SFD, respectively. Both plots are presented on a carbon-equivalent basis. The contribution of O_2 to the total TEA flux becomes progressively more important with increasing SFD, from 35% at 100 m to 100% at 5000 m SFD. However, O_2 contributes less than 10% to the C_{ox} rate at 100 m SFD (Figure 6b) because most is used to oxidize reduced metabolites (see section 3.3). The contribution of NO_3^- to the TEA flux and C_{ox} rate is less variable, being around 5–10% in both cases which agrees with previous estimates [*Middelburg et al.*, 1996]. Iron oxide contributes only <1% of the TEA and C_{ox} rate, and that of manganese reduction is an order of magnitude lower (data not shown). Because the depositional fluxes of iron and manganese oxide are poorly constrained, the significance of these latter values is uncertain, and important contributions of iron and manganese reduction may be highly localized [*Canfield et al.*, 1993; *Van Cappellen and Wang*, 1996]. Around 60% of total carbon oxidation potential between 100 and 2000 m is supplied by SO_4^{2-} (Figure 6a), yet in situ sulfide oxidation leads to sulfate-based carbon mineralization rates which contribute ~80% to the total C_{ox} rate at these depths. The relative importance of SO_4^{2-} decreases sharply below 2000 m, and at 5000 m SO_4^{2-} is not used in carbon mineralization.

[32] Globally integrated fluxes and carbon mineralization rates are presented in Table 4. The continental shelf between 0 and 150 m, corresponding to ~6% of the seafloor (Table 1), is responsible for 52% of global sulfate reduction (8 Tmol SO_4^{2-} yr^{-1}) and 45% of the global TOU of 21 Tmol yr^{-1}. Considering that TOU is equivalent to POC flux and ignoring the small loss of ODU released as N_2 during denitrification (~3% of total carbon equivalents), the inner shelf thus also receives 45% of the global deposition flux of POC. The continental shelf as a whole is responsible for 55% of total O_2 uptake and 64% of sulfate reduction. This compares to 61% and 64%, respectively, for the shelf (0–200 m) calculated by *Jørgensen and Kasten* [2006] for the data compiled by *Canfield* [1993] and *Canfield et al.* [2005]. The shelf is also highly significant for reactive iron input (84% of total flux) and reduction rates (83% of total). Denitrifi-

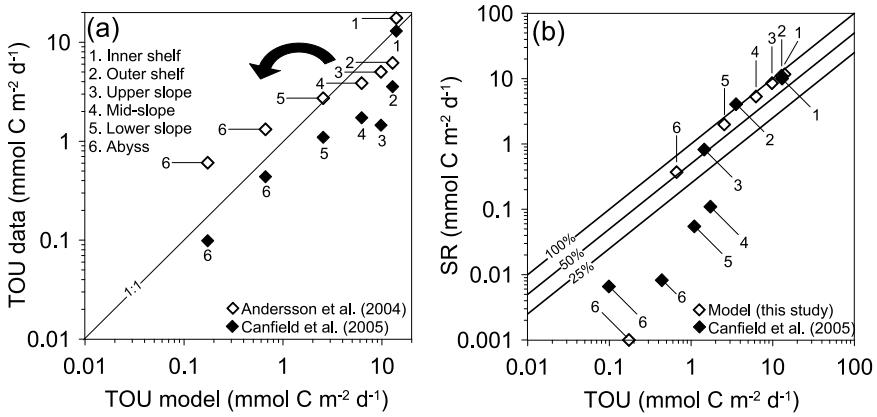

Figure 7. (a) Experimentally derived TOU data grouped according to ocean margin type from two literature sources versus TOU data derived for the reaction-transport model approach. The arrow indicates possible downslope transport of carbon from the shelf in nepheloid layers. (b) Rates of sulfate reduction converted to carbon units by multiplying by 2 versus TOU data grouped according to ocean margin type. The black diamonds are data from *Canfield et al.* [2005] modified after *Jørgensen and Kasten* [2006], and the white diamonds are model data. No sulfate reduction is predicted for the deep abyss by the model, and this point is located on the TOU axis.

cation, on the other hand, is more evenly distributed throughout the ocean, with 34% taking place on the shelf, 29% on the slope and 37% in the abyss. Over half of all denitrification occurs at SFD below 1500 m by virtue of the large expanse of slope and abyssal sediments. Denitrification removes around 1.1 Tmol NO_3^- yr^{-1} from the ocean, which is less than 1.6–2 Tmol yr^{-1} calculated by the model of *Middelburg et al.* [1996], who considered the degradable POC to consist of two pools with different reactivity. In the deepest SFD interval, comprising 48% of the seafloor, oxidation of reduced biogenic nitrogen sustains a small efflux of NO_3^- from the sediment equivalent to 2% of global benthic NO_3^- uptake. Further, because the POM reaching the seafloor is particularly recalcitrant (Table 3), these deep abyssal sediments consume only 11% of the global O_2 flux.

[33] Further insight into the model performance can be gained by comparison with the literature TOU data (Figure 7a). Even though the relative TOU distribution with SFD discussed above compares well to other studies, it can be seen that the model predicts higher values than those observed by *Andersson et al.* [2004] for the outer shelf and midslope to upper slope and lower values for the lower slope and the abyss. Additionally, the model always predicts higher TOU than predicted by *Canfield et al.* [2005]. The implications of this are twofold. First, assuming that the true TOU lies somewhere between the Canfield and Andersson models, the global statistical relationship for quantifying reactive carbon fluxes based on SFD (equation (17)) provides a reasonable estimate of integrated C_{ox} rates for the inner shelf and deep ocean, but over predicts the rate for water depths either side of the shelf break. This could be due to the downslope transport of POM and the focusing of organic-rich material from the shelf in nepheloid layers [*Inthorn et al.*, 2006]. Second, *Andersson et al.* [2004] predict higher TOU than *Canfield et al.* [2005] by a factor of 1.2 for the shelf and a factor of 100 for the abyss. There are considerable differences, therefore, both for the TOU predicted by the model and the data, and for the various TOU directly derived from observations.

[34] Despite the discrepancies, our global TOU estimate (21 Tmol yr^{-1}, Table 4) is comparable to the experimentally derived values of 23 Tmol yr^{-1} by *Canfield et al.* [2005], 19 Tmol yr^{-1} by *Jørgensen* [1983] and 22 Tmol yr^{-1} by *Smith and Hollibaugh* [1993]. The SFD-dependent parameters thus provide a reasonable estimate of global carbon deposition. Sulfate reduction accounts for 76% of the global carbon mineralization rate (16 Tmol yr^{-1}) and aerobic respiration only for 15% (3.1 Tmol yr^{-1}). The remainder is mainly attributed to denitrification (6%) and iron reduction (3%). Therefore, although the fluxes of O_2 and SO_4^{2-} into the sediment are 10 Tmol yr^{-1} and 5.5 Tmol yr^{-1}, which are equal to 10 Tmol yr^{-1} and 11 Tmol yr^{-1} on a carbon oxidation capacity, respectively, SO_4^{2-} actually plays a much larger role in carbon mineralization because of the diversion of O_2 to oxidize H_2S (see section 3.3). In fact, our model results suggest that sulfate-based carbon mineralization plays a more important role

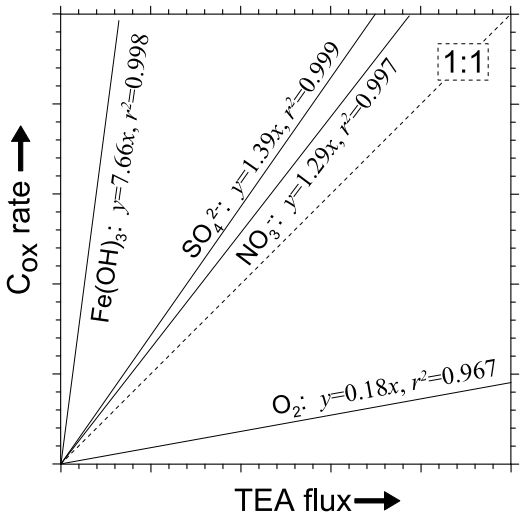

Figure 8. Modeled depth-integrated C_{ox} rates by each TEA as a function of the TEA flux into the sediment for all modeled SFD. The data are taken from Figure 5, where the TEA fluxes have been converted to carbon equivalent units. To simplify, the data are plotted on an arbitrary scale, and only the linear regression curves are shown.

in global benthic carbon oxidation than previously reported. For instance, the data compiled by *Canfield* [1993] and *Canfield et al.* [2005] gives a sulfate-based contribution of 55–65% [*Canfield et al.*, 2005; *Jørgensen and Kasten*, 2006]. Moreover, *Archer et al.* [2002] suggested that aerobic respiration is the dominant respiration pathway at all SFDs, accounting for 66% of total carbon mineralization. The higher rates of sulfate reduction are also evident in Figure 5e, where modeled rates (10–100 μmol cm^{-2} yr^{-1}) are greater than the values reported in the *Middelburg et al.* [1997] database (0.1–20 μmol cm^{-2} yr^{-1}).

[35] It is important to resolve these discrepancies because they imply a major revision of the role of O_2 versus SO_4^{2-} in global carbon cycling in the seafloor. Further analysis of the model data shows where the differences in the estimates originate. The depth-resolved data of sulfate-based carbon mineralization are plotted in Figure 7b against TOU and compared to the data set of *Canfield et al.* [2005]. The straight lines on the log-log plot represent contributions of sulfate reduction to total carbon oxidation of 25, 50 and 100%. The values corresponding to water depths down to the upper slope (<750 m) for both our model and the *Canfield et al.* [2005] data fall between the upper two straight lines, which implies that sulfate reduction accounts for between 50 and 100% of total carbon mineralization. For the midslope down to parts of the abyss (SFD between 750 and 4250 m), amounting to > 40% of the ocean floor (Table 1), the model continues to predict a high contribution of sulfate-based carbon mineralization (55–85%) except for the deep abyss, whereas *Canfield et al.* [2005] predict a sharp decrease to 6%. It is interesting to point out that if the model-predicted TOU for the midslope and below (8 Tmol yr^{-1}, Table 4) is partitioned between aerobic respiration and sulfate reduction such that the latter accounts for 6% of TOU instead of up to 85%, then the global contribution of sulfate reduction falls to 56%, i.e., similar to the estimations of *Canfield et al.*, 2005 and *Jørgensen and Kasten* [2006]. Consequently, it would appear that it is the contribution from the deep sea sulfate reduction predicted by the model (SFD range from 2750 to 4250 m) which inflates the global estimate of sulfate-based carbon mineralization.

3.3. Secondary Redox Cycling

[36] In this section, the cycling of TEAs, and reduced species (NH_4^+, Mn^{2+}, Fe^{2+} and H_2S) and the resulting ODUs is investigated in more detail. The model-derived data across the SFD intervals are synthesized into a normalized plot of C_{ox} rate versus TEA flux, both axes presented on a carbon-equivalent basis (Figure 8). The 1:1 line indicates equal TEA fluxes and C_{ox} rates. The C_{ox} rate for each primary redox pathway is positively correlated with the total flux of TEA into the sediment. No correlation was obtained for MnO_2. For O_2, the rate of aerobic respiration is a factor of 5 smaller that the O_2 flux (slope = 0.18). In contrast, the C_{ox} rates using NO_3^-, $Fe(OH)_3$ and SO_4^{2-} are larger than 1. In situ production of NO_3^-, $Fe(OH)_3$ and SO_4^{2-} through oxidation of NH_4^+, Fe^{2+}, FeS and H_2S by O_2 explains these observations. This is clearly an important source of SO_4^{2-}, considering the large contribution of sulfate reduction to carbon respiration (Figure 6 and Table 4). The steep slope for $Fe(OH)_3$ reflects intense recycling within the sediment, and indicates that each iron atom is recycled about 8 times before burial or transport back to the water column. The production of NO_3^- from biogenic nitrogen (i.e., NH_4^+) occurs at all SFD, and the slope of 1.29 indicates that biogenic nitrogen is a significant source of NO_3^- but remains quantitatively less important by a factor of 4 than the influx of NO_3^- from the ocean. The fraction of the depth-integrated denitrification rate supported by biogen-

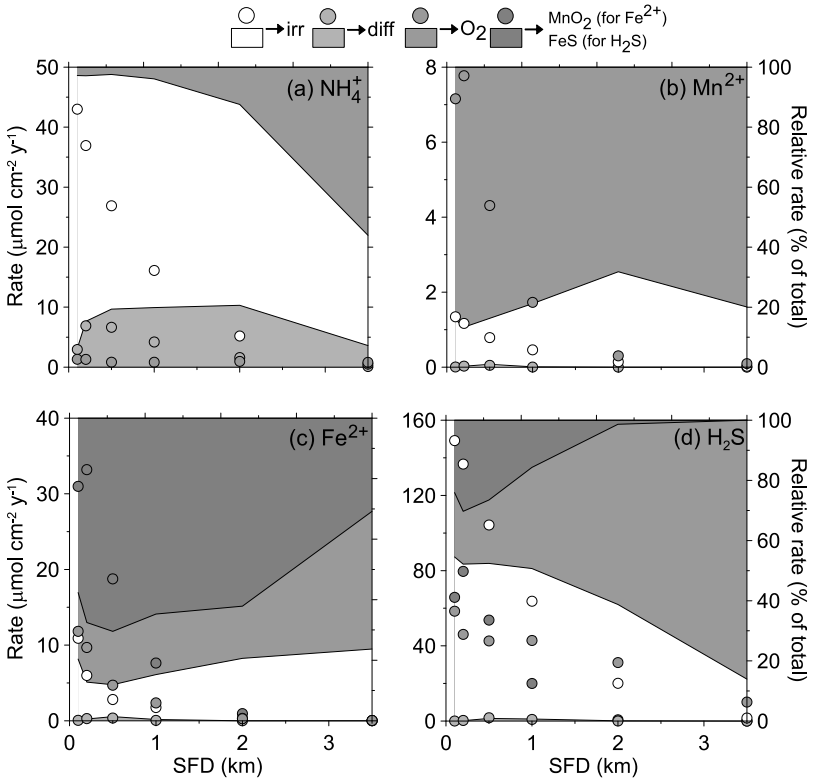

Figure 9. Absolute (symbols) and relative (shading) losses of (a) NH_4^+, (b) Mn^{2+}, (c) Fe^{2+}, and (d) H_2S along the global hypsometry. Sinks indicated at the top include oxidation by O_2, diffusion from the sediment to the ocean, nonlocal transport out of the sediment by bioirrigation, and oxidation by MnO_2 (for Fe^{2+}) and precipitation into FeS (for H_2S).

ic nitrogen may be significantly higher in oxygen minimum zones over the continental margins [*Devol*, 1991; *Archer et al.*, 2002]. Data compiled by *Canfield* [1993] seem to suggest that when O_2 availability falls below ~20 μM a greater fraction of carbon oxidation occurs with NO_3^-. These low concentrations are not globally representative, however, and in our simulations O_2 was always above 100 μM.

[37] The sink pathways of NH_4^+, Mn^{2+}, Fe^{2+} and H_2S with SFD are shown in Figure 9 as relative and absolute values. The data exclude the 5000 m SFD interval because the high O_2 penetration depth (Figure 2b) prohibits significant production of these reduced species in the surface sediments. Major sinks on shelf and slope sediments (SFD < 2000 m) include bioirrigation out of the sediment for NH_4^+ and H_2S, and oxidation for Mn^{2+} and Fe^{2+}. Losses by diffusion across the sediment-water interface are only important for NH_4^+. Precipitation of FeS accounts for 30% of the H_2S sink in shallow water depths, yet as precipitation takes place in the bioturbated zone 99% of the FeS is subsequently reoxidized to sulfate by O_2 (resulting in maximum concentrations of buried FeS around 10 μmol g^{-1} at shallow SFD; data not shown). The reoxidation of Fe^{2+} to $Fe(OH)_3$ by MnO_2 demonstrates a close coupling of the manganese and iron cycles. Relatively less Fe^{2+} is oxidized by O_2 because MnO_2 is the first oxidant encountered by Fe^{2+} as it diffuses upward. The model does not consider Fe^{2+} oxidation by NO_3^-, which may also compete with MnO_2 for Fe^{2+} [*Dhakar and Burdige*, 1996].

[38] It is important to note that direct losses of H_2S to the ocean by diffusion and bioirrigation are a significant sink of reducing equivalents throughout most of the ocean (Figure 9d). This ODU loss is equivalent to 11 Tmol O_2 yr^{-1} (Table 4), and means that DOU measurements would account for 50% of TOU. The additional flux of NH_4^+ originating from PON, which is not included in the ODU flux value in Table 4, is equal to 3.2 Tmol O_2 yr^{-1}. It is thus remarkable that approximately half of the oxygen demand which enters the

sediment as POC is lost from the sediment by efflux to the ocean as ODU. This effect decreases with SFD (Figure 9) because higher O_2 penetration effectively traps the ODUs in the sediment by oxidation and prevents their escape to the water column. This important result requires that the imposed rate of bioirrigation determined from semiempirical statistical functions [*Meile and Van Cappellen*, 2003] and, more importantly, the irrigation attenuation with depth (3.5 cm^{-1} assumed constant throughout the ocean) are realistic. If the irrigation depth is too high, then H_2S will be flushed from the system and escape in situ oxidation. While data from the oligotrophic Bermuda Time Series site suggest that diffusion dominates solute transport in the deep sea [*Sayles and Martin*, 1995], *Glud et al.* [1994] observed that TOU exceeded DOU in deep Atlantic sediments by 1–3 times. In this case though, they attributed the excess oxygen uptake to the formation of oxic surfaces on burrow walls as well as respiration by the animals rather than sulfide escape. The fact remains that reliable and spatially resolved data of irrigation depths calculated using geochemical tracers (e.g., Br^-) in the different biogeochemical provinces of the seafloor [e.g., *Seiter et al.*, 2005] is not available. It is our view that this is currently the largest obstacle to be surmounted before a global assessment of subsurface solute transport and nonlocal solute exchange with bottom waters can be made.

[39] The results nevertheless allow us to speculate on the role of bioirrigation in more practical terms. On the basis of benthic chamber TOU experiments, it has been argued that up to 95% of sulfide produced in marine sediments is oxidized to sulfate [*Jørgensen*, 1977a, 1977b]. This figure is derived from mass balance closure of the sulfur cycle as the difference between sulfur burial and sulfate reduction. Our model provides further insight into the sulfur cycle, and predicts that 30% of sulfide (as H_2S and FeS) is oxidized in situ, with the remainder lost to the ocean by bioirrigation of H_2S. Laying aside for the moment the concerns over the depth-integrated bioirrigation rate, if this sulfide were to be rapidly oxidized in the overlying water then by mass balance closure our model would predict that close to 100% of sulfide is oxidized and that a large fraction of the O_2 flux (76%) is involved in the reoxidation of sulfide. It is generally assumed that the contribution to TOU by sulfide oxidation takes place in the oxic and suboxic surface sediment layers, although on the basis of the model results presented here we would argue that the largest proportion is oxidized above the sediment. Dissolved sulfide is not routinely measured in chambers, although *Linke et al.* [2005] showed that sulfide may not become detectable until O_2 is depleted. Rapid chemical sulfide oxidation by O_2 [*Millero et al.*, 1987; *Buisman et al.*, 1990] could potentially maintain very low concentrations of sulfide above the seafloor and disguise the sulfide irrigation flux. Again, more information on irrigation depths would resolve this issue definitively.

3.4. Uncertainty of Model Predictions

[40] The presented model predictions (as is the case for model predictions in general) are subject to uncertainties introduced during the model design and parameterization. Simplifications in model structure concern the choice of the reaction network and the description of transport and reaction processes which inadvertently lead to idealized representations of reality. For instance, nutrients such as phosphorus [e.g., *Katsev et al.*, 2006] or trace elements [e.g., *Canavan et al.*, 2007] are excluded from the reaction network. This choice was guided by the lack of evidence for a major, global control of these species on the primary and secondary redox reactions investigated here. Precipitation/dissolution processes of alkaline earth metal minerals [e.g., *Luff and Wallmann*, 2003; *Arndt et al.*, 2006], adsorption kinetics [e.g., *Van Cappellen and Wang*, 1996], and redox reactions involved in methane cycling [e.g., *Dale et al.*, 2008a, 2008b] are ignored here. The dissolved concentration of iron and manganese may nevertheless be affected directly or indirectly by precipitation or sorption, but because of the high uncertainty in the boundary conditions for metal oxides, it was chosen to ignore the influence of these additional processes on iron and manganese cycling. Furthermore, methanogenesis only really needs to be considered when combined with the degradation of refractory carbon at larger sediment depths, and is considered to account for 5% of total carbon mineralization [*Jørgensen and Kasten*, 2006].

[41] Simplifications concerning the rate laws are primarily centered on the 1-G description of the carbon degradation model. This approach is conceptually attractive since more complex formulations require additional parameters which are

unknown in the context of global-scale applications. The 1-G model neglects, however, the very labile organic material which is decomposed close to the sediment surface as well as the recalcitrant carbon pools present at large sediments depths. The degradation of these highly reactive and refractory pools would have opposite effects on the relative contribution of the various metabolic pathways of organic matter decomposition. Higher rates near the SWI would steepen oxygen profiles and, thus, promote higher oxygen fluxes and aerobic degradation rates. Carbon oxidation at large depth would lead to increased sulfate-reduction rates and, eventually, to the onset of methanogenesis and methane oxidation [*Dale et al.*, 2008b]. A decrease of POM oxidation rate for the different degradation pathways along the redox gradient would have similar effects. Yet, the overall quantitative effect of these additional carbon pools on redox cycling cannot currently be predicted at the global scale. It is, however, likely that the results will ultimately depend on choice of which carbon degradation model (e.g., multi-G [*Westrich and Berner*, 1984]; power law [*Middelburg*, 1989]; reactive continuum [*Boudreau and Ruddick*, 1991; *Tromp et al.*, 1995]) is most adequate to describe the complexity of organic matter degradation [e.g., *Brüchert and Arnosti*, 2003]. Furthermore it has not yet been determined whether model predictions would be affected by the explicit inclusion of microbial biomass into reaction kinetics as suggested elsewhere [*Wirtz*, 2003; *Thullner et al.*, 2005, 2007].

[42] Uncertainties have also been introduced during the implementation of transport processes and include the assumption of constant porosity and the use of simplified functional dependencies to define bioirrigation and bioturbation intensities with depth. As in the upper most part of the sediment the latter two processes have been shown here to be dominant for species transport, whereas the variations in advection through burial triggered by porosity changes will only have a minor impact on the model results. It should be noted that the volume of the solid matrix can change significantly due to porosity variations but the combined effect of porosity and bioturbation on the distribution of solid species is not straightforward [*Mulsow et al.*, 1998] even though bioturbation is dominant in the uppermost part of the sediment. *Teal et al.* [2008] showed that global-scale estimates for bioturbation depths and intensities are subject to high uncertainties caused among others by measurement results depending on the applied experimental method and by sampling sites unevenly distributed at the global scale. An increase in bioturbation is assumed to shift carbon degradation activities toward larger sediment depths, a process which would favor sulfate reduction over aerobic degradation [*Meysman et al.*, 2005]. Bioirrigation is a major transport process for dissolved species, especially at shallow SFD (Figure 4). In the absence of bioirrigation, the dominance of sulfate reduction would even be more pronounced (results not shown). Higher bioirrigation rates than those used here would increase the supply of oxygen to the sediment, hence favoring aerobic degradation.

[43] All parameters used in this study are subject to uncertainties. Intuitively, model results should be most sensitive to variations in parameters that are directly controlling the fluxes of POM and TEAs as well as the rate of organic carbon oxidation. For instance, using a power law dependency instead of an exponential dependency of POM fluxes on SFD as done previously [e.g., *Middelburg et al.*, 1997] and also adopted in this study would lead to a greater contribution of deep sea sediments to global carbon oxidation and to much higher global carbon mineralization rates [*Glud*, 2008] than reported elsewhere. Consequently, the contribution of the different degradation pathways at the global scale would be altered. However, advanced sensitivity analyses of complex nonlinear systems have revealed that a priori ranking of parameters concerning the associated uncertainty of model results is not recommendable [e.g., *Holstein and Wirtz*, 2009]. Detailed and systematic sensitivity analyses should thus be performed in the future to determine if the most poorly constrained parameters (e.g., depth of irrigation and bioturbation, carbon reactivity, boundary conditions for iron and manganese and rate constants for secondary reaction rates) are also the largest sources of uncertainty for the shown model results. Future research should also address how the uncertainly in model prediction could be reduced most, especially whether more detailed models depending on a large number of poorly constrained parameters are better suited than simplified models depending on less, better constrained parameter values when it comes to improving confidence in model predictions.

3.5. Synthesis and Implications

[44] Using a reaction-transport model approach, we have quantified the global benthic carbon mineralization in the seafloor (21 Tmol C yr^{-1}). This flux, assumed to be equivalent to carbon-based TOU, is in good agreement with previous experimental estimates of TOU on a global basis and in satisfactory agreement with TOU estimates on a depth-resolved basis. This lends support a controversial finding of this study, that is, carbon degradation is dominated by sulfate reduction at all SFD except in the deep abyss. The global contribution of sulfate-based POC mineralization (76%) is higher than previous estimates (25–65%) because of the higher contribution from deep sea sediments (~2750–4250 m). Aerobic respiration becomes increasingly important with SFD, yet accounts for only 15% of global POC mineralization. Higher rates of aerobic mineralization at the expense of sulfate reduction would bring our model predictions of sulfate-based carbon mineralization into line with the literature.

[45] Current estimates of integrated sulfate reduction rates for the deep sea, where sulfate penetrates 10^1–10^2 m, are mainly inferred from the diffusive flux calculated from deep sea drilling project (DSDP) pore water concentration profiles well below the surface [*Canfield et al.*, 2005]. This provides an estimate for net sulfate reduction rates and is only valid if no production or consumption occurs over the linear concentration gradient from which the flux is calculated. Sulfide oxidation in reducing microenvironments within the sulfate reduction zone [*Jørgensen*, 1977b] or by reactive iron mineral phases [*Raiswell and Canfield*, 1996] could lead to an underestimation of sulfate reduction rates calculated in this way. Our model provides an additional indication that sulfate reduction could be occurring in deep sea sediments relatively close to the sediment-water interface where sulfate concentration profiles are vertical (Figure 2d). Detection of sulfate reduction from dissolved sulfide concentrations may also not be possible because of sulfide trapping into iron sulfides followed by mixing into the suboxic surface layers by bioturbation and reoxidization. This could potentially allow sulfate reduction to bypass visual inspection or even experimental detection [*Froelich et al.*, 1979]. Along similar lines, the strikingly linear sulfate concentration profiles in slope sediments of the southeast Atlantic published by *Fossing et al.* [2000] and attributed to bioirrigation of sulfate suggests much lower rates of sulfate reduction than were measured by ^{35}S incubation studies. A careful assessment of sulfate reduction rates in lower slope and abyssal sediments, if at all possible using current analytical methodologies given the above complicating factors, should be viewed as a research priority.

[46] All the above brings into question previous results which show that 100 to 1000 times more POC is oxidized by O_2 than by sulfate in deep sea sediments [*Canfield et al.*, 2005]. *Mackin and Swider* [1989] used an analytical model to determine the controls on aerobic respiration versus sulfate reduction. Through sensitivity analysis, they noted that respiration of C_{org} by O_2 will only exceed 20% of C_{ox} if (1) the reactive carbon attenuates rapidly with depth, (2) C_{ox} is very low, and (3) bioturbation is prevalent. These effects will increase the penetration of oxygen in the sediment and, consequently, the oxygen exposure time (OET). Increased OET enhances C_{org} degradation [*Hartnett et al.*, 1998], and so will reduce the fraction degraded by sulfate. Implementation of the OET concept in the model can be done simply by defining a higher rate constant (equation (18)) for aerobic mineralization [*Tromp et al.*, 1995] or by including an additional labile pool of C_{org} [*Middelburg et al.*, 1996; *Soetaert et al.*, 1996; *Archer et al.*, 2002]; see also section 3.4. Our view is that first resolving the discrepancies in irrigation depth and deep-sea sulfate reduction rates is needed before addressing the question of the appropriate carbon degradation model.

4. Summary and Conclusions

[47] In the present study early diagenetic processes in marine sediments and the resulting fluxes of reactive species were simulated using a reactive transport modeling approach. Using the SFD as master variable and defining globally averaged environmental conditions as input data for the simulation of individual SFD intervals resulted in realistic concentration and reaction rate profiles inside the sediment. When making a SFD resolved comparison between experimental data presented in the literature and simulated sediment depth integrated carbon oxidation rates and fluxes of species across the sediment-water interface, some quantitative discrepancies between our

Table A1. Primary C_{ox} Pathways, Stoichiometries, and Rate Laws r_n Implemented in the Reaction Network[a]

Pathway	Stoichiometry	Reaction Rate (per Mol Carbon)
Aerobic degradation	$(CH_2O)_x(NH_3)_y(H_3PO_4)_z + (x + 2y)O_2 + (y + 2z)HCO_3^- \rightarrow (x + y + 2z)CO_2 + yNO_3^- + zHPO_4^{2-} + (x + 2y + 2z)H_2O$	$r_{O2} = k_C \cdot c_{CH2O} \cdot f_{O2}$
Denitrification	$5(CH_2O)_x(NH_3)_y(H_3PO_4)_z + (4x + 3y)NO_3^- \rightarrow (2x + 4y)N_2 + (x - 3y + 10z)CO_2 + (4x + 3y - 10z)HCO_3^- + 5zHPO_4^{2-} + (3x + 6y + 10z)H_2O$	$r_{NO3} = k_C \cdot c_{CH2O} \cdot f_{NO3}$
Manganese reduction	$(CH_2O)_x(NH_3)_y(H_3PO_4)_z + 2xMnO_2 + (3x + y - 2z)CO_2 + (x + y - 2z)H_2O \rightarrow 2xMn^{2+} + (4x + y - 2z)HCO_3^- + yNH_4^+ + zHPO_4^{2-}$	$r_{MnO2} = k_C \cdot c_{CH2O} \cdot f_{MnO2}$
Iron reduction	$(CH_2O)_x(NH_3)_y(H_3PO_4)_z + 4xFe(OH)_3 + (7x + y - 2x)CO_2 \rightarrow 4xFe^{2+} + (8x + y - 2z)HCO_3^- + yNH_4^+ + zHPO_4^{2-} + (3x - y + 2z)H_2O$	$r_{FeOH3} = k_C \cdot c_{CH2O} \cdot f_{FeOH3}$
Sulfate reduction	$2(CH_2O)_x(NH_3)_y(H_3PO_4)_z + xSO_4^{2-} + 2(y - 2z)CO_2 + 2(y - 2z)H_2O \rightarrow xH_2S + 2(x + y - 2z)HCO_3^- + 2yNH_4^+ + 2zHPO_4^{2-}$	$r_{SO4} = k_C \cdot c_{CH2O} \cdot f_{SO4}$

[a] Here, f_n is defined as $f_n = \left(1 - \sum_{j<n} f_j\right) \cdot 1$ if $c_n > K_n$ and $f_n = \left(1 - \sum_{j<n} f_j\right) \cdot \frac{c_n}{K_n}$ if $c_n < K_n$. The index n refers to the TEA used in each organic carbon decomposition pathway, K_n denotes the corresponding half-saturation constant (see Table A3), and k_c is a first-order rate constant. The Redfield ratio x/y/z is set to 106/12/1. Phosphate concentration changes are not included into the simulations.

results and these previous estimates can be observed. This might be attributed to simplifications made in our simulations approach. Nevertheless, the simulated results on global fluxes and their changes with SFD are in general agreement with previous estimates supporting the validity of our approach.

[48] The results of our study indicate that in marine sediments at the global-scale sulfate reduction might be a more important organic oxidation pathway than previously assumed. Although the deep abyss is characterized by mainly aerobic conditions, the high total oxidation rates in shelf sediments results in these shallow (mainly sulfate reducing) SFD being responsible for most of the global carbon oxidation and resulting fluxes of redox species. Furthermore, bioirrigation is a major contributor to dissolved species fluxes across the sediment-water interface. This indicates that flux estimates based on diffusion profiles might lead to an underestimation of species fluxes. Bioirrigation also allows reduced species to be transported back to the water column before their reoxidation in the sediment. This can lead to an inequality between net oxygen uptake into the sediments and total carbon oxidation rates and thus to a potential underestimation of carbon oxidation rates in marine sediments if they are derived from dissolved oxygen uptake.

[49] Future steps to improve the validity of the model predictions on global mineralization pathways and species fluxes would include a regionalization of the SFD-parameter relations used in this study. This regionalization should focus mainly on shelf sediments, as these sediments contribute most to the global rates and species fluxes and are most affected by terrestrial and climatic influences resulting in a higher variability than observed for deeper SFD. In addition, more experimental data on the relevance of bioirrigation and of individual carbon oxidation pathways at various environmental conditions would help to improve our understanding of these sediment systems and their contribution to global element cycles.

Appendix A: Reaction Network and Reaction Rate Parameters

[50] Tables A1 and A2 provide a list of stoichiometries and rate laws for all reactions implemented in the model (reaction network from *Van Cappellen and Wang* [1995]). Parameter values for the reac-

Table A2. Secondary Redox Reactions, Nonredox Mineral Precipitation/Dissolution, and Acid-Base Equilibria Implemented in the Reaction Network Showing Stoichiometries and Rate Laws r_l for the Kinetic Processes[a]

	Stoichiometry	Reaction Rate
R1	$NH_4^+ + 2O_2 + 2HCO_3^- \rightarrow NO_3^- + 2CO_2 + 3H_2O$	$r_1 = k_1 \cdot c_{NH4} \cdot c_{O2}$
R2	$Mn^{2+} + 1/2O_2 + 2HCO_3^- \rightarrow MnO_2 + 2CO_2 + H_2O$	$r_2 = k_2 \cdot c_{Mn2} \cdot c_{O2}$
R3	$Fe^{2+} + 1/4O_2 + 2HCO_3^- + 1/2H_2O \rightarrow Fe(OH)_3 + 2CO_2$	$r_3 = k_3 \cdot c_{Fe2} \cdot c_{O2}$
R4	$2Fe^{2+} + MnO_2 + 2HCO_3^- + 2H_2O \rightarrow 2Fe(OH)_3 + Mn^{2+} + 2CO_2$	$r_4 = k_4 \cdot c_{Fe2} \cdot c_{MnO2}$
R5	$H_2S + 2O_2 + 2HCO_3^- \rightarrow SO_4^{2-} + 2CO_2 + 2H_2O$	$r_5 = k_5 \cdot c_{O2} \cdot (c_{HS} + c_{H2S})$
R6	$H_2S + MnO_2 + 2CO_2 \rightarrow Mn^{2+} + S^0 + 2HCO_3^-$	$r_6 = k_6 \cdot c_{MnO2} \cdot (c_{HS} + c_{H2S})$
R7	$H_2S + 2Fe(OH)_3 + 4CO_2 \rightarrow 2Fe^{2+} + S^0 + 4HCO_3^- + H_2O$	$r_7 = k_7 \cdot c_{FeOH3} \cdot (c_{HS} + c_{H2S})$
R8	$FeS + O_2 \rightarrow Fe^{2+} + SO_4^{2-}$	$r_8 = k_8 \cdot c_{FeS} \cdot c_{O2}$
R9	$Mn^{2+} + 2HCO_3^- \rightarrow MnCO_3 + CO_2 + H_2O$	$r_9 = \left(\begin{array}{l} k_9^+ \cdot H^* \left(\frac{c_{Mn2} \cdot c_{CO3}}{K_{S,MnCO3}} - 1 \right) \\ + k_9^- \cdot c_{MnCO3} \cdot \left(1 - H^* \left(\frac{c_{Mn2} \cdot c_{CO3}}{K_{S,MnCO3}} - 1 \right) \right) \end{array} \right) \cdot \left(\frac{c_{Mn2} \cdot c_{CO3}}{K_{S,MnCO3}} - 1 \right)$
R10	$Fe^{2+} + 2HCO_3^- \rightarrow FeCO_3 + CO_2 + H_2O$	$r_{10} = \left(\begin{array}{l} k_{10}^+ \cdot H^* \left(\frac{c_{Fe2} \cdot c_{CO3}}{K_{S,FeCO3}} - 1 \right) \\ + k_{10}^- \cdot c_{FeCO3} \cdot \left(1 - H^* \left(\frac{c_{Fe2} \cdot c_{CO3}}{K_{S,FeCO3}} - 1 \right) \right) \end{array} \right) \cdot \left(\frac{c_{Fe2} \cdot c_{CO3}}{K_{S,FeCO3}} - 1 \right)$
R11	$Fe^{2+} + H_2S + 2HCO_3^{2-} \rightarrow FeS + 2CO_2 + 2H_2O$	$r_{11} = \left(\begin{array}{l} k_{11}^+ \cdot H^* \left(\frac{c_{Fe2} \cdot c_{HS}}{c_H \cdot K_{S,FeS}} - 1 \right) \\ + k_{11}^- \cdot c_{FeS} \cdot \left(1 - H^* \left(\frac{c_{Fe2} \cdot c_{HS}}{c_H \cdot K_{S,FeS}} - 1 \right) \right) \end{array} \right) \cdot \left(\frac{c_{Fe2} \cdot c_{HS}}{c_H \cdot K_{S,FeCO3}} - 1 \right)$
R12	$H^+ + HCO_3^- \leftrightarrow CO_2 + H_2O$	thermodynamic equilibrium
R13	$H^+ + CO_3^{2-} \leftrightarrow HCO_3^-$	thermodynamic equilibrium
R14	$H^+ + HS^- \leftrightarrow H_2S$	thermodynamic equilibrium

[a] (R1)–(R8), secondary redox reactions; (R9)–(R11), nonredox mineral precipitation/dissolution; (R12)–(R14), acid-base equilibria. H^* is the Heaviside operator with $H^*(x) = 1$ for $x \geq 0$, and $H^*(x) = 0$ for $x < 0$. k_l ($l = 1, \ldots 11$) denote all reaction rate parameters.

Table A3. SFD Dependency of Parameter Values Used in Reaction Rate Laws[a]

	Seafloor Depth						
	100 m	200 m	500 m	1000 m	2000 m	3500 m	5000 m
Reaction rate parameters							
k_c (yr^{-1})	0.221	0.208	0.174	0.130	0.0718	0.0296	0.0122
k_1 (M^{-1} yr^{-1})	1.5×10^7	1.5×10^7	1.0×10^7	1.0×10^7	1.0×10^7	1.0×10^7	1.0×10^7
k_2 (M^{-1} yr^{-1})	2.0×10^9	2.0×10^9	1.0×10^9	1.0×10^9	1.0×10^9	1.0×10^9	1.0×10^9
k_3 (M^{-1} yr^{-1})	2.0×10^9	2.0×10^9	1.0×10^9	1.0×10^9	1.0×10^9	1.0×10^9	1.0×10^9
k_4 (M^{-1} yr^{-1})	2.46×10^8	2.00×10^8	1.08×10^8	3.84×10^7	4.88×10^6	2.21×10^5	1.00×10^4
k_5 (M^{-1} yr^{-1})	6.0×10^8	6.0×10^8	3.0×10^8	3.0×10^8	3.0×10^8	3.0×10^8	3.0×10^8
k_6 (M^{-1} yr^{-1})	1.0×10^4	1.0×10^4	1.0×10^4	1.0×10^4	1.0×10^4	1.0×10^4	1.0×10^4
k_7 (M^{-1} yr^{-1})	1.0×10^4	1.0×10^4	1.0×10^4	1.0×10^4	1.0×10^4	1.0×10^4	1.0×10^4
k_8 (M^{-1} yr^{-1})	2.2×10^7	2.2×10^7	2.0×10^7	2.0×10^7	2.0×10^7	2.0×10^7	2.0×10^7
k_9^+ (mol/(g y))	1.15×10^{-6}	1.00×10^{-6}	6.49×10^{-7}	3.16×10^{-7}	7.50×10^{-8}	8.66×10^{-9}	1.00×10^{-9}
k_9^- (yr^{-1})	2.50×10^{-1}	2.22×10^{-1}	1.14×10^{-1}	7.03×10^{-2}	1.72×10^{-2}	2.07×10^{-3}	2.50×10^{-4}
k_{10}^+ (mol/(g yr))	1.15×10^{-6}	1.00×10^{-6}	6.49×10^{-7}	3.16×10^{-7}	7.50×10^{-8}	8.66×10^{-9}	1.00×10^{-9}
k_{10}^- (yr^{-1})	2.50×10^{-1}	2.22×10^{-1}	1.14×10^{-1}	7.03×10^{-2}	1.72×10^{-2}	2.07×10^{-3}	1.00×10^{-3}
k_{11}^+ (mol/(g y))	5.97×10^{-6}	5.00×10^{-6}	2.93×10^{-6}	1.21×10^{-6}	2.05×10^{-7}	1.43×10^{-8}	1.00×10^{-9}
k_{11}^- (yr^{-1})	1.00×10^{-3}	8.69×10^{-4}	5.69×10^{-4}	2.81×10^{-4}	6.87×10^{-5}	8.29×10^{-6}	1.00×10^{-6}
Half-saturation constants for OCO reactions							
K_{O2} (μM)	8	8	8	8	8	8	8
K_{NO3} (μM)	10	10	10	10	10	10	10
K_{MnO2} (μmol g^{-1})	2	2	2	2	2	2	2
K_{FeOH3} (μmol g^{-1})	5	5	5	5	5	5	5
K_{SO4} (μM)	1000	1000	2000	2000	2000	2000	2000

[a] Adapted from *Van Cappellen and Wang* [1995].

tion rate laws are given in Table A3 as function of the seafloor depth (SFD).

Acknowledgments

[51] This study was funded by the Netherlands Organization for Scientific Research (NWO) grant 813.02.008. Additional financial support has been provided to M.T. by the Helmholtz Association grant VG-NG 338 (GReaT MoDE) and to P.R. by the NWO-VIDI grant 864.05.007 and the government of the Brussels-Capital region (Brains Back to Brussels award). We also appreciated helpful comments from Philippe Van Cappellen and from the reviewers of this manuscript (Sergei Katsev and Stephen Meyers).

References

Aguilera, D. R., P. Jourabchi, C. Spiteri, and P. Regnier (2005), A knowledge-based reactive transport approach for the simulation of biogeochemical dynamics in Earth systems, *Geochem. Geophys. Geosyst.*, *6*, Q07012, doi:10.1029/2004GC000899.

Aller, R. C. (1994), The sedimentary Mn cycle in Long Island Sound: Its role as intermediate oxidant and the influence of bioturbation, O_2, and C_{org} flux on diagenetic reaction balances, *J. Mar. Res.*, *52*, 259–295, doi:10.1357/0022240943077091.

Andersson, J. H., J. W. M. Wijsman, P. M. J. Herman, J. J. Middelburg, K. Soetaert, and C. Heip (2004), Respiration patterns in the deep ocean, *Geophys. Res. Lett.*, *31*, L03304, doi:10.1029/2003GL018756.

Archer, D. E., J. L. Morford, and S. R. Emerson (2002), A model of suboxic sedimentary diagenesis suitable for automatic tuning and gridded global domains, *Global Biogeochem. Cycles*, *16*(1), 1017, doi:10.1029/2000GB001288.

Arndt, S., H.-J. Brumsack, and K. Wirtz (2006), Cretaceous black shales as active bioreactors: A biogeochemical model for the deep biosphere encountered during ODP Leg 207 (Demerara Rise), *Geochim. Cosmochim. Acta*, *70*, 408–425, doi:10.1016/j.gca.2005.09.010.

Berelson, W. M., D. E. Hammond, D. O'Neil, X. M. Xu, C. Chin, and J. Zukin (1990), Benthic fluxes and pore water studies from sediments of the central equatorial North Pacific: Nutrient diagenesis, *Geochim. Cosmochim. Acta*, *54*, 3001–3012, doi:10.1016/0016-7037(90)90117-4.

Berelson, W. M., J. McManus, K. H. Coale, K. S. Johnson, T. Kilgore, D. Burdige, and C. Pilskaln (1996), Biogenic matter diagenesis on the sea floor: A comparison between two continental margin transects, *J. Mar. Res.*, *54*, 731–762, doi:10.1357/0022240963213673.

Berg, P., S. Rysgaard, and B. Thamdrup (2003), Dynamic modeling of early diagenesis and nutrient cycling: A case study in an Arctic marine sediment, *Am. J. Sci.*, *303*, 905–955, doi:10.2475/ajs.303.10.905.

Berner, R. A. (1980), *Early Diagenesis: A Theoretical Approach*, Princeton Univ. Press, Princeton, N. J.

Boudreau, B. P. (1996), A method-of-lines code for carbon and nutrient diagenesis in aquatic sediments, *Comput. Geosci.*, *22*, 479–496, doi:10.1016/0098-3004(95)00115-8.

Boudreau, B. P. (1997), *Diagenetic Models and Their Implementation*, Springer, Berlin.

Boudreau, B. P., and B. R. Ruddick (1991), On a reactive continuum representation of organic-matter diagenesis, *Am. J. Sci.*, *291*, 507–538.

Brüchert, V., and C. Arnosti (2003), Anaerobic carbon transformation: Experimental studies with flow through cells, *Mar. Chem.*, *80*, 171–183, doi:10.1016/S0304-4203(02)00119-6.

Buisman, C., P. Uspeert, A. Janssen, and G. Lettinga (1990), Kinetics of chemical and biological sulphide oxidation in aqueous solutions, *Water Res.*, *24*, 667–671, doi:10.1016/0043-1354(90)90201-G.

Burdige, D. J. (2006), *Geochemistry of Marine Sediments*, Princeton Univ. Press, Princeton, N. J.

Cai, W.-J., and C. E. Reimer (1995), Benthic oxygen flux, bottom water oxygen concentration and core top organic carbon content in the deep northeast Pacific Ocean, *Deep Sea Res., Part A*, *42*, 1681–1699, doi:10.1016/0967-0637(95)00073-F.

Canavan, R. W., P. Van Cappellen, J. J. G. Zwolsman, G. A. van den Berg, and C. P. Slomp (2007), Geochemistry of trace metals in fresh water sediment: Field results and diagenetic modeling, *Sci. Total Environ.*, *381*, 263–279, doi:10.1016/j.scitotenv.2007.04.001.

Canfield, D. E. (1989), Sulfate reduction and oxic respiration in marine sediments: Implications for organic-carbon preservation in euxinic environments, *Deep Sea Res., Part A*, *36*, 121–138, doi:10.1016/0198-0149(89)90022-8.

Canfield, D. E. (1993), Organic matter oxidation in marine sediments, in *Interactions of C, N, P and S Biogeochemical Cycles and Global Change*, *NATO ASI Ser., Ser. I*, vol. 4, edited by R. Wollast, F. T. Mackenzie, and L. Chou, pp. 333–364, Springer, Berlin.

Canfield, D. E., B. Thamdrup, and J. Hansen (1993), The anaerobic degradation of organic matter in Danish coastal sediments: Iron reduction, manganese reduction, and sulfate reduction, *Geochim. Cosmochim. Acta*, *57*, 3867–3883, doi:10.1016/0016-7037(93)90340-3.

Canfield, D. E., B. Thamdrup, and E. Kristensen (2005), *Aquatic Geomicrobiology*, *Adv. Mar. Biol.*, vol. 48, Elsevier Acad., Amsterdam.

Conkright, M. E., R. A. Locarnini, H. E. Garcia, T. D. O'Brien, T. P. Boyer, C. Stephens, and J. I. Antonov (2002), *World Ocean Atlas 2001: Objective Analyses, Data Statistics, and Figures*, CD-ROM documentation, Natl. Oceanogr. Data Cent., Silver Spring, Md.

Dale, A. W., D. R. Aguilera, P. Regnier, H. Fossing, N. J. Knab, and B. B. Jørgensen (2008a), Seasonal dynamics of the depth and rate of anaerobic oxidation of methane in Aarhus Bay (Denmark) sediments, *J. Mar. Res.*, *66*, 127–155, doi:10.1357/002224008784815775.

Dale, A. W., P. Regnier, N. J. Knab, B. B. Jørgensen, and P. Van Cappellen (2008b), Anaerobic oxidation of methane (AOM) in marine sediments from the Skagerrak (Denmark): II. Reaction-transport modelling, *Geochim. Cosmochim. Acta*, *72*, 2880–2894, doi:10.1016/j.gca.2007.11.039.

Dale, A. W., V. Brüchert, M. Alperin, and P. Regnier (2009), An integrated sulfur isotope model for Namibian shelf sediments, *Geochim. Cosmochim. Acta*, *73*, 1924–1944, doi:10.1016/j.gca.2008.12.015.

Devol, A. H. (1991), Direct measurement of nitrogen gas fluxes from continental shelf sediments, *Nature*, *349*, 319–321, doi:10.1038/349319a0.

Dhakar, S. P., and D. J. Burdige (1996), A coupled, non-linear, steady state model for early diagenetic processes in pelagic sediments, *Am. J. Sci.*, *296*, 296–330.

Ferdelman, T. G., H. Fossing, K. Neumann, and H. D. Schulz (1999), Sulfate reduction in surface sediments of the southeast Atlantic continental margin between 15°38′S and 27°57′S (Angola and Namibia), *Limnol. Oceanogr.*, *44*, 650–661.

Fossing, H., T. G. Ferdelman, and P. Berg (2000), Sulfate reduction and methane oxidation in continental margin sediments influenced by irrigation (south-east Atlantic off Namibia), *Geochim. Cosmochim. Acta*, *64*, 897–910.

Froelich, P. N., G. P. Klinkhammer, M. L. Bender, N. A. Luedtke, G. R. Heath, D. Cullen, and P. Dauphin (1979), Early oxidation of organic matter in pelagic sediments of the eastern equatorial Atlantic: Suboxic diagenesis, *Geochim. Cosmochim. Acta*, *43*, 1075–1090, doi:10.1016/0016-7037(79)90095-4.

Glud, R. N. (2008), Oxygen dynamics of marine sediments, *Mar. Biol. Res.*, *4*, 243–289, doi:10.1080/17451000801888726.

Glud, R. N., J. K. Gundersen, B. B. Jorgensen, N. P. Revsbech, and H. D. Schulz (1994), Diffusive and total oxygen uptake of deep-sea sediments in the eastern South Atlantic Ocean: In situ and laboratory measurements, *Deep Sea Res., Part II*, *41*, 1767–1788, doi:10.1016/0967-0637(94)90072-8.

Hammond, D. E., J. McManus, W. M. Berelson, T. E. Kilgore, and R. H. Pope (1996), Early diagenesis of organic material in equatorial Pacific sediments: Stoichiometry and kinetics, *Deep Sea Res., Part II*, *43*, 1365–1412, doi:10.1016/0967-0645(96)00027-6.

Hartnett, H. E., R. G. Keil, J. I. Hedges, and A. H. Devol (1998), Influence of oxygen exposure time on organic carbon preservation in continental margin sediments, *Nature*, *391*, 572–574, doi:10.1038/35351.

Hensen, C., H. Landenberger, M. Zabel, and H. D. Schulz (1998), Quantification of diffusive benthic fluxes of nitrate, phosphate and silicate in the southern Atlantic Ocean, *Global Biogeochem. Cycles*, *12*, 193–210, doi:10.1029/97GB02731.

Hensen, C., M. Zabel, and H. N. Schulz (2006), Benthic cycling of oxygen, nitrogen and phosphorus, in *Marine Geochemistry*, edited by H. D. Schulz and M. Zabel, pp. 207–234, Springer, Heidelberg, Germany.

Holstein, J. M., and K. Wirtz (2009), Sensitivity analysis of nitrogen and carbon cycling in marine sediments, *Estuarine Coastal Shelf Sci.*, *82*, 632–644, doi:10.1016/j.ecss.2009.02.008.

Inthorn, M., V. Mohrholz, and M. Zabel (2006), Nepheloid layer distribution in the Benguela upwelling area offshore Namibia, *Deep Sea Res., Part I*, *53*, 1423–1438, doi:10.1016/j.dsr.2006.06.004.

Jahnke, R. A. (1996), The global ocean flux of particulate organic carbon: Areal distribution and magnitude, *Global Biogeochem. Cycles*, *10*, 71–88, doi:10.1029/95GB03525.

Jahnke, R. A., C. E. Reimers, and D. B. Craven (1990), Intensification of recycling of organic matter at the sea floor near ocean margins, *Nature*, *348*, 50–54, doi:10.1038/348050a0.

Jørgensen, B. B. (1977a), The sulfur cycle of a coastal marine sediment (Limfjorden, Denmark), *Limnol. Oceanogr.*, *22*, 814–832.

Jørgensen, B. B. (1977b), Bacterial sulfate reduction within reduced microniches of oxidized marine sediments, *Mar. Biol. Berlin*, *41*, 7–17, doi:10.1007/BF00390576.

Jørgensen, B. B. (1982), Mineralization of organic matter in the sea bed—The role of sulfate reduction, *Nature*, *296*, 643–645, doi:10.1038/296643a0.

Jørgensen, B. B. (1983), Processes at the sediment-water interface, in *The Major Biogeochemical Cycles and Their Interactions*, edited by B. Bolin and R. C. Cook, pp. 477–509, Sci. Comm. on Problems of the Environ., Paris.

Jørgensen, B. B., and S. Kasten (2006), Sulfur cycling and methane oxidation, in *Marine Geochemistry*, edited by

H. D. Schulz and M. Zabel, pp. 271–302, Springer, Heidelberg, Germany.

Jourabchi, P., P. Van Cappellen, and P. Regnier (2005), Quantitative interpretation of pH distributions in aquatic sediments: A reaction-transport modeling approach, *Am. J. Sci.*, *305*, 919–956, doi:10.2475/ajs.305.9.919.

Katsev, S., I. Tsandev, I. L'Heureux, and D. G. Rancourt (2006), Factors controlling long-term phosphorous efflux from lake sediments: Exploratory reactive-transport modeling, *Chem. Geol.*, *234*, 127–147, doi:10.1016/j.chemgeo.2006.05.001.

Linke, P., K. Wallmann, E. Suess, C. Hensen, and G. Rehder (2005), In situ benthic fluxes from an intermittently active mud volcano at the Costa Rica convergent margin, *Earth Planet. Sci. Lett.*, *235*, 79–95.

Longhurst, A., S. Sathyendranath, and T. Platt (1995), An estimate of global primary production in the ocean from satellite radiometer data, *J. Plankton Res.*, *17*, 1245–1271, doi:10.1093/plankt/17.6.1245.

Luff, R., and L. Wallmann (2003), Fluid flow, methane fluxes, carbonate precipitation and biogeochemical turnover in gas hydrate-bearing sediments at Hydrate Ridge, Cascadia Margin: Numerical modeling and mass balances, *Geochim. Cosmochim. Acta*, *67*, 3403–3421, doi:10.1016/S0016-7037(03)00127-3.

Mackin, J. E., and K. T. Swider (1989), Organic-matter decomposition pathways and oxygen consumption in coastal marine sediments, *J. Mar. Res.*, *47*, 681–716, doi:10.1357/002224089785076154.

Meile, C., and P. Van Cappellen (2003), Global estimates of enhanced solute transport in marine sediments, *Limnol. Oceanogr.*, *48*, 777–786.

Meile, C., C. M. Koretsky, and P. Van Cappellen (2001), Quantifying bioirrigation in aquatic sediments: An inverse modeling approach, *Limnol. Oceanogr.*, *46*, 164–177.

Meile, C., P. Berg, P. Van Cappellen, and K. Tuncay (2005), Solute-specific pore water irrigation: Implications for chemical cycling in early diagenesis, *J. Mar. Res.*, *63*, 601–621.

Meysman, F. J. R., O. S. Galaktionov, S. Madani, and J. J. Middelburg (2005), Modeling biological interactions in aquatic sediments as coupled reactive transport, in *Interactions Between Macro- and Microorganisms in Marine Sediments*, *Coastal Estuarine Stud.*, vol. 60, edited by E. Kristensen et al., pp. 359–388, AGU, Washington, D. C.

Middelburg, J. J. (1989), A simple model for organic matter decomposition in marine sediments, *Geochim. Cosmochim. Acta*, *53*, 1577–1581, doi:10.1016/0016-7037(89)90239-1.

Middelburg, J. J., K. Soetaert, P. M. J. Herman, and C. H. R. Heip (1996), Denitrification in marine sediments: A model study, *Global Biogeochem. Cycles*, *10*, 661–673, doi:10.1029/96GB02562.

Middelburg, J. J., K. Soetaert, and P. M. J. Herman (1997), Empirical relationships for use in global diagenetic models, *Deep Sea Res., Part I*, *44*, 327–344, doi:10.1016/S0967-0637(96)00101-X.

Millero, F. J., S. Hubinger, M. Fernandez, and S. Garnett (1987), Oxidation of H_2S in seawater as a function of temperature, pH, and ionic strength, *Environ. Sci. Technol.*, *21*, 439–443, doi:10.1021/es00159a003.

Mulsow, S., B. P. Boudreau, and J. N. Smith (1998), Bioturbation and porosity gradients, *Limnol. Oceanogr.*, *43*, 1–9.

National Geophysical Data Center (1993), 5-minute gridded global relief data (ETOPO5), *NGDC Data Announce. 93-MGG-01*, Boulder, Colo.

Raiswell, R., and D. E. Canfield (1996), Rates of reaction between silicate iron and dissolved sulfide in Peru Margin sediments, *Geochim. Cosmochim. Acta*, *60*, 2777–2787, doi:10.1016/0016-7037(96)00141-X.

Regnier, P., J. P. O'Kane, C. I. Steefel, and J. P. Vanderborght (2002), Modeling complex multi-component reactive transport systems: Towards a simulation environment based on the concept of a Knowledge Base, *Appl. Math. Model.*, *26*, 913–927, doi:10.1016/S0307-904X(02)00047-1.

Reimers, C. E., R. A. Jahnke, and D. C. McCorkle (1992), Carbon fluxes and burial rates over the continental slope and rise off central California with implications for the global carbon cycle, *Global Biogeochem. Cycles*, *6*, 199–224, doi:10.1029/92GB00105.

Sayles, F. L., and W. R. Martin (1995), In situ tracer studies of solute transport across the sediment-water interface at the Bermuda Time Series site, *Deep Sea Res., Part I*, *42*, 31–52, doi:10.1016/0967-0637(94)00033-O.

Seiter, K., C. Hensen, and M. Zabel (2005), Benthic carbon mineralization on a global scale, *Global Biogeochem. Cycles*, *19*, GB1010, doi:10.1029/2004GB002225.

Slomp, C. P., J. F. P. Malschaert, L. Lohse, and W. Van Raaphorst (1997), Iron and manganese cycling in different sedimentary environments on the North Sea continental margin, *Cont. Shelf Res.*, *17*, 1083–1117, doi:10.1016/S0278-4343(97)00005-8.

Smith, S. V., and J. T. Hollibaugh (1993), Coastal metabolism and the oceanic organic carbon balance, *Rev. Geophys.*, *31*, 75–89, doi:10.1029/92RG02584.

Soetaert, K., P. M. J. Herman, and J. J. Middelburg (1996), A model of early diagenetic processes from the shelf to abyssal depths, *Geochim. Cosmochim. Acta*, *60*, 1019–1040, doi:10.1016/0016-7037(96)00013-0.

Teal, L. R., M. T. Bulling, E. R. Parker, and M. Solan (2008), Global patterns of bioturbation intensities and mixed depth of marine soft sediments, *Aquat. Biol.*, *2*, 207–218.

Thamdrup, B. P., and D. E. Canfield (1996), Pathways of carbon oxidation in continental margin sediments off central Chile, *Limnol. Oceanogr.*, *41*, 1629–1650.

Thullner, M., P. Van Cappellen, and P. Regnier (2005), Modeling the impact of microbial activity on redox dynamics in porous media, *Geochim. Cosmochim. Acta*, *69*, 5005–5019, doi:10.1016/j.gca.2005.04.026.

Thullner, M., P. Regnier, and P. Van Cappellen (2007), Modeling microbially induced carbon degradation in redox-stratified subsurface environments: Concepts and open questions, *Geomicrobiol. J.*, *24*, 139–155, doi:10.1080/01490450701459275.

Tromp, T. K., P. Van Cappellen, and R. M. Key (1995), A global model for the early diagenesis of organic carbon and organic phosphorus in marine sediments, *Geochim. Cosmochim. Acta*, *59*, 1259–1284, doi:10.1016/0016-7037(95)00042-X.

Van Cappellen, P., and J.-F. Gaillard (1996), Biogeochemical dynamics in aquatic sediments, in *Reactive Transport in Porous Media*, *Rev. Mineral.*, vol. 34, P. C. Lichtner, C. I. Steefel, and E. H. Oelkers, pp. 335–376, Mineral. Soc. of Am., Washington, D. C.

Van Cappellen, P., and Y. Wang (1995), Metal cycling in surface sediments: Modeling the interplay or transport and reaction, in *Metal Speciation and Contamination of Aquatic Sediments*, edited by H. E. Allen, pp. 21–64, Ann Arbor Press, Chelsea, Mich.

Van Cappellen, P., and Y. Wang (1996), Cycling of iron and manganese in surface sediments: A general theory for the coupled transport and reaction of carbon, oxygen, nitrogen, sulfur, iron, and manganese, *Am. J. Sci.*, *296*, 197–243.

Westrich, J. T., and R. A. Berner (1984), The role of sedimentary organic matter in bacterial sulfate reduction: The G model tested, *Limnol. Oceanogr.*, *29*, 236–249.

Wijsman, J. W. M. (2000), Early diagenetic processes in northwestern Black Sea sediments, Ph.D. thesis, Groningen Univ., Groningen, Netherlands.

Wirtz, K. (2003), Control of biogeochemical cycling by mobility and metabolic strategies of microbes in the sediments: An integrated model study, *FEMS Microbiol. Ecol.*, *46*, 295–306, doi:10.1016/S0168-6496(03)00196-X.

Zabel, M., and C. Hensen (2006), Quantification and regionalization of benthic fluxes, in *Marine Geochemistry*, edited by H. D. Schulz and M. Zabel, pp. 429–452, Springer, Heidelberg, Germany.